

SILICON NANOCRYSTAL DOPED POLYMER NANOWIRE ARRAYS

A THESIS

SUBMITTED TO THE DEPARTMENT OF PHYSICS

AND THE GRADUATE SCHOOL OF ENGINEERING AND SCIENCE

OF BILKENT UNIVERSITY

IN PARTIAL FULFILLMENT OF THE REQUIREMENTS

FOR THE DEGREE OF

MASTER OF SCIENCE

By

Muhammet Çelebi

August, 2013

I certify that I have read this thesis and that in my opinion it is fully adequate, in scope and in quality, as a thesis for the degree of Master of Science.

Assoc. Prof. Dr. Mehmet Bayındır (Advisor)

I certify that I have read this thesis and that in my opinion it is fully adequate, in scope and in quality, as a thesis for the degree of Master of Science.

Assoc. Prof. Dr. Selçuk Aktürk

I certify that I have read this thesis and that in my opinion it is fully adequate, in scope and in quality, as a thesis for the degree of Master of Science.

Assoc. Prof. Dr. Ceyhun Bulutay

Approved for the Graduate School of Engineering and Science:

Prof. Dr. Levent Onural
Director of the Graduate School

ABSTRACT

SILICON NANOCRYSTAL DOPED POLYMER NANOWIRE ARRAYS

Muhammet Çelebi

M.S. in Physics

Supervisor: Assoc. Prof. Dr. Mehmet Bayındır

August, 2013

In this thesis, we successfully produced silicon nanocrystal embedded polymer micro and nanowire arrays by using a new top-to-bottom nanofabrication approach. Silicon nanocrystal (Si-Nc) quantum dots are photoluminescent materials that give bright optical illumination under UV light excitation. Si-Ncs were used to fabricate large area luminescent thin polymer films before production of the fibers. Among many of Si-Nc fabrication methods that are available, we chose a chemical route which takes the advantage of high product yield and ease of production steps, although the resultant size distribution is not uniform as other methods such as electrochemical treatment of Si wafers. Dopant Si-Ncs in polymer sheets shows some improved properties compared to free standing silicon nanocrystals, like longer luminescent life time in normal atmospheric conditions and in high temperatures as high as 300 °C. With utilizing these properties, thermal drawing of Si-Nc doped polymer fibers is possible without harming the luminescence properties. Hence, throughout the work, different types of films were investigated and polycarbonate films were chosen for both their thermal and optical properties such as durable luminescence at high temperatures and low absorption at visible wavelengths. Consequently, with combining these properties with our iterative thermal size reduction method, we successfully produced silicon nanocrystal doped polymer micro and nanowire arrays.

In literature, there are similar works treating the same idea of producing luminescent fibers, which were realized with different techniques and material sets, like dye/QD doped nanofibers or fibers produced with conjugated polymers. However, the methods used to produce these type of geometries lacks in some aspects such as limited length, uniformity, alignment, reproducibility, *etc.* On the other hand, our iterative thermal drawing method is very successful for producing indefinitely long, uniform and easily aligned fibers. Our production steps can be

summed in five steps which are: Si-Nc synthesis, film preparation, film-rolling, consolidation, and two consecutive fiber drawing.

Keeping the track of characterization of the product in each step is important. Hence, for silicon nanocrystals, we took photoluminescence (PL) intensity measurements, SEM/TEM images and temperature dependent PL measurements. Also for doped films, we performed temperature dependent PL measurements and for the resultant fibers we carried out cross-section SEM and PL characterizations.

Silicon nanocrystal embedded micro and nanowires can be utilized as fiber gain medium, single photon source, directional emitter, light emitting diodes and optical sensing elements. Also, they increase light extraction efficiencies with guiding advantages and this can result to fluorescence enhancement for luminescent active material dopants.

Keywords: Silicon nanocrystals, nanotechnology, quantum dots, nanowires, fiber optics, polymer fibers, iterative size reduction.

ÖZET

SİLİKON NANOKRİSTAL GÖMÜLÜ POLİMER NANOTEL DİZİLER

Muhammet Çelebi

Fizik, Yüksek Lisans

Tez Yöneticisi: Assoc. Prof. Dr. Mehmet Bayındır

Ağustos, 2013

Bu tezde, silikon nanokristallerin sentezlenmesi ve yeni bir nano-üretim tekniğiyle silikon nanokristal katkılı mikro ve nanotellerin üretilmesi, incelenmiştir. Silikon kuantum noktalar ya da nanokristaller, UV ışık uyarımıyla görünür dalga boyunda parlak ışık yayan yapılardır. Bir çok nanokristal üretim metodu içinde, biz çok fazla son ürün vermesi ve üretim kolaylığı sebebiyle, kimyasal yolları tercih ettik. Polimere gömülmüş silikon nanokristaller, gömülmeyenlere nazaran bazı gelişmiş özellikler gösterebilirler. Örneğin; oda koşullarında ve 300 °C gibi yüksek sıcaklıklarda dahi uzun süre ışımalı kalma bunlardan bir tanesidir. Bu özelliklerinden yararlanılarak tekrarlamalı olarak ısı fiber çekme işleminde kullanılmaları mümkün olmaktadır. Dolayısıyla, bu çalışma boyunca bir kaç farklı polimer film denenmiş ve optik ve ısı özelliklerinden dolayı polikarbon filmde karar kılınmıştır. Bunlardan yola çıkarak görülüyor ki çalışma grubumuzda sıkça kullanılan tekrarlamalı ısı fiber çekme yöntemiyle silikon nanokristal gömülmüş nanofiberler üretmek mümkündür ve sonuçlarımız ve ürünlerimiz bunu desteklemektedir.

Literatürde silikon nanokristal gömülü ya da konjuge polimerle üretilen bazı çalışmalar bulunmakla birlikte bu çalışmaların hizalama, tekrarlanamama, üretim zorluğu gibi bazı dezavantajları bulunmaktadır. Bunlarla beraber bu çalışmadakine benzer şekilde ısı yöntemlerle üretilen bazı çalışmalar da vardır ancak bizim çalışmamız nano boyuta inmesi ve üretim aşamalarının farklılığıyla bu çalışmalardan ayrılmakta hatta bazı avantajlarıyla bir kaç adım öne geçmektedir. Örneğin, tekrarlamalı yöntemle ürettiğimiz fiberlerin kolay hizalanabilme, yeknesanlık ve çok uzun boyluluk gibi avantajları vardır. Üretim yöntemimiz, nanokristal sentezi, ince film hazırlama, sarma ve katılaştırma ve fiber çekmeden oluşmaktadır.

Ortaya çıkan ara ürünlerin karakterizasyonlarının takip edilebilmesi, çalışmanın gelişmesi açısından önemlidir. Dolayısıyla, her adımda elde edilen örnekler detaylı bir şekilde gerekli görülen ölçümlere tabi tutulmuşlardır. Bu ölçümler ışıma yoğunluğu ölçümü ve TEM/SEM resimleri olarak sayabiliriz. Ayrıca, gömülü filmler için sıcaklığa bağlı ışıma yoğunluğu değişimi ölçümü de yapılmıştır. Son olarak, elde edilen fiberlerin ara kesit resimleri ve ışımaları yoğunluk ölçümleriyle birlikte alınmıştır.

Bu çalışma sonunda elde edilen silikon nanokristal gömülü fiberler, fiber kazanç ortamı, tek foton kaynağı, yönelimli yayıcı, ışık yayan diyotlar ve optik sensörler olarak kullanılabilirler. Ayrıca, yönlendirme özelliklerinden dolayı da belirli yönlerde ışıma yoğunluğunu artırma özelliği de gösterebilirler.

Anahtar sözcükler: Silikon nanokristaller, nanoteknoloji, kuantum noktalar, fiberiçi yapılar, nanoteller, fiber optik, polimer fiberler, tekrarlamalı boyut küçültme tekniği.

Acknowledgement

First, I would thank to my thesis advisor Mehmet Bayındır for his invaluable advice, uninterrupted support since my undergraduate study. Also, I am thankful to my group colleagues M. Halit Dolaş, Mehmet Kanık, Tural Khudiyev, Ozan Aktaş, Hülya Budunoglu, Murat Dere, Dr. Gokcen Birlik Demirel and Dr. Osama Tobail. Also, I am thankful to Salim Çıracı for his great vision and effort to built such a great research center UNAM.

I also gratefully acknowledge that UNAM and the financial support from TÜBİTAK.

Last but not least, I would like to thank my fiancée, Elif, for her love, kindness and support she has shown during the past two years it has taken me to finalize this thesis.

Contents

1	Introduction	1
2	Quantum Dots and Embedded Designs	4
2.1	Quantum Dots and Applications	5
2.2	Active Material Embedded Luminescent Fibers	12
2.3	Fabrication Techniques for Producing Nanostructures	18
3	Synthesis and Characterization of Silicon Quantum Dots and Silicon Nanocrystal Doped Polymer Films	24
3.1	Silicon Nanocrystals	25
3.2	Synthesis and Characterization of Silicon Nanocrystals	29
3.3	Large-Area Silicon Nanocrystal Doped Thin Films	34
4	Silicon Nanocrystals Embedded Micro- and Nano-Structures	41
4.1	Preparation of Macroscopic Preform	42
4.2	Production of Core-Shell Nanowires by Iterative Size Reduction Technique	47

<i>CONTENTS</i>	ix
4.3 Characterization of Nanostructures	55
5 Summary and Outlook	64
A Data	79
B Code	80

List of Figures

2.1	Quantum dots with vivid colours spanning from violet to deep red.	5
2.2	Exciton generation with the combination of an excited electron and a hole.	6
2.3	Size-energy band relationship in semiconductor quantum dots. Energy levels begin to split when the dimension of the nanocrystal quantum dot becomes to be on the order of its exciton-Bohr radius. Also, with decreasing size, the bandgap widens hence the luminescence shifts toward smaller wavelengths.	8
2.4	Schematic representations of quantum dot types. (a) Core types generally consist of two different elements which constitute crystal structure together. (b) Core/Shell type includes two different type of crystal structure built from different content crystals. (c) For alloyed quantum dots, ternary alloys can be homogenous distribution or a gradient through the volume.	9
2.5	Some representative examples from applications of quantum dots.	12
2.6	An example of QD doped electrospun polymer nanofibers: Some of the results presented by Schlect <i>et al.</i>	13
2.7	Dye/QDs doped electrospun polymer nanofibers produced by Tomzcak <i>et al.</i>	15

2.8	Light emitting fiber FET and electroluminescent fiber designs. . .	16
2.9	All optical display designs and surface emitting fiber laser.	17
2.10	Schematic diagram of electrospinning process. With applying a high voltage difference, molecules in the solution both polarized and subsequently accelerated toward the target. With a continuous supply of both solution and electric field, fibers can be constructed on the target.	19
2.11	Schematic illustration of nanofibers fabrication by direct drawing method	20
2.12	Schematic illustration of thermal drawing process. Size of the materials showing glass properties can be reduced with simultaneous application of heat and force. This results to size reduction in perpendicular directions to drawing forces while increment in parallel directions.	21
2.13	QD doped fiber production with in-situ generation	22
3.1	Diamond lattice of silicon nanocrystal. Thermal annealing of the HSQ molecular precursor leads to formation of nanocrystalline silicon that has diamond lattice. The final size of the crystal is dependent on experimental conditions.	25
3.2	Some representative examples from silicon nanocrystal embedded applications.	28
3.3	Synthesis of silicon nanocrystals. The synthesis starts with annealing of the HSQ precursor, following with grinding for further size reduction and uniform size distribution and finally with chemical etching, luminescent nanocrystals are held. Etching time determines the resulting coloration. Also, initial size distribution is effective for determination of etching time requirements.	30

- 3.4 (a) Computer controlled high temperature furnace used for annealing the precursor molecules of silicon nanocrystals. (b) Auto-mortar used for grinding resulting silicon nanocrystal powder after high temperature annealing and (c) the powder after treatment. 31
- 3.5 Measured PL intensity of silicon nanocrystals dispersed in pentane. The peak corresponds to red color. Also, the shape of the curve is measure of relative size distribution. In other words, there are nanocrystals emitting other colors rather than red but their number is small comparing to red emitting nanocrystals. 32
- 3.6 (a) High Resolution TEM image of silicon nanocrystals in surrounding SiO₂ matrix. Crystal sites can be seen in yellow circles. The regular patterns corresponds to crystalline silicon whereas irregular patterns belongs to amorphous glass matrix. (b) Corresponding electron diffraction pattern of crystalline silicon. The rings corresponds to distances between lattice planes. 33
- 3.7 Measured PL intensities of free standing silicon nanocrystals on a quartz wafers with varying temperature from different samples. (Temperatures are in centigrade (°C) degrees.) (a) The first sample prepared by dip-coating method. (b) The second sample prepared by same method and from same Si-Nc solution. Increasing temperature initially decreases the intensity then it shifts toward smaller wavelengths and increases, which is known as blue shift. The difference between two figures may be due to samples which they are dip-coated. The size distribution hence oxidation rate is not same for two samples. However, their tendency and behaviour are similar eventhough it is not exactly same. 35
- 3.8 Schematic representation of the doped thin film production. Corresponding solution of the desired content is poured into the rectangular mold. Then, doped thin films are yielded after waiting for the evaporation of the solvents. 37

3.9	Image of silicon nanocrystal doped thin polycarbonate film under UV illumination. Red color of the film is due to dopant silicon nanocrystals where the excitation wavelength was 325 nm. The scale bar corresponds to 3 cm.	38
3.10	Measured PL intensities of the doped film with varying temperature and corresponding photographic images (inset). PL intensities increases up to 175 °C then reduces, with increasing temperature. The trend can be seen in photographic image. However, another phenomena known as blue shift takes place when the temperature reaches to 175 °C. Also, the maximum of the measured intensities occurs at 150 °C, which is thought to be due to refractive index change of the surrounding polymer which has glass transition around 150 °C.	40
4.1	Schematic illustrations of cross sections of the designed fibers. The geometries consist of core/cladding structure and a thin PVDF layer for protection of the core during chemical etching of the cladding	43
4.2	Rectangular doped core preform. (a) Bright field image of the core and (b) UV image of the same. Red luminescence can be seen in latter image which shows consolidation process does not harm luminescence of the silicon nanocrystals	44
4.3	Subdivided and carved PC preform. Rectangular carved regions are adjusted to just fit to doped core. (a) Image of the preform with doped core placed in the hole. (b) Capped of the same. (c) UV image of the same.	45
4.4	Consolidated rectangular doped core preform and final form of it which is stucked to adopter preform before drawing.	46

4.5	Schematic representation of cylindrical doped core preparation. The first three steps are doped film preparation as explained before. Doped preform preparation steps are cutting doped films into circular pieces, filling them into a cylindrical glass mold, consolidation and removing the mold.	47
4.6	Images of the silicon nanocrystal doped PC core preform. (a) Bright field image of the core. (b) UV image of the same. (c) Another doped core preform obtained from the post-etching method which causes red color to turn into yellow. (d) Another UV image of the core preforms	48
4.7	Preparation of a preform. Several layers of thin polymer films are tightly rolled around the doped core until the desired dimensions are held. Then, with thermally treating this structure, it is consolidated and becomes the final form before drawing.	48
4.8	Final form of the cylindrical doped core structure and corresponding sizes. (a) Consolidated preform. (b) Corresponding core/cladding dimensions.	49
4.9	Computer controlled fiber tower facility and its schematic diagram	50
4.10	Illustrative drawing explaining the parameters of thermal drawing. The parameters are defined as in the text.	51
4.11	Schematic illustration of iterative thermal drawing technique. With repeated procedure its is possible to get kilometers long, nanofibers. Here another crucial property is the array structure. The array can consist of hundreds of antecedent fibers.	53
4.12	The first step fibers. (a) Bright field microscope image of rectangular doped core fiber and (b) SEM image of cylindrical fiber. . .	54
4.13	SEM image of cross-section of second step doped fiber. In the second step, doped core diameters were reduced to nanodimensions.	55

4.14	Highly ordered first step fibers that are thermally drawn and their red luminescent UV image. In the inset the luminescent core can be seen. This non-complex geometry is important for applications which needs precise and simple control.	57
4.15	Cross sections of first step fibers. (a) UV image of cylindrical core fiber. (b) UV image of rectangular core. Bright red colors can be seen at the core regions.	58
4.16	Measured PL intensity of the cylindrical core fiber. The peak positioned at 610nm and it proofs orange-like color of the first step fibers.	59
4.17	Images of aligned and colored Si-Nc doped polymer fibers. (a) The institute's name is written with luminescent cores. The image shows alignment ability of the fibers. (b) Green colored fibers which resulted from red luminescent fibers by HF etching treatment. (c) Yellow colored fibers which are also fabricated by a similar treatment but for a lesser treatment time.	60
4.18	Luminescent microscope images and measured PL intensity of second step fibers. (a) UV image of second step fibers. Discrete luminescent points are the nanocrystal sites. (b) Corresponding luminescence measurement of second step fibers. There is difference in peak positions of the first and the second step fibers, which is probably due to samples gotten from different sections of the first step fibers.	62
4.19	SEM images of second step fibers. (a) Side view. At some points, fiber geometries are distorted due to crystal size larger than fiber diameter. However, it still shows the applicability of the technique. (b) Cross-section of a second step fiber showing hexagonal packed array of antecedent step fibers.	63

5.1 Iron nanoparticle doped films, preforms and fibers produced with the methods used in this work. The images shows that the methods are also suitable for other type of dopants and polymers rather than material sets used in this work. (Courtesy of Dr. Gökçen Birlik Demirel) 68

List of Tables

2.1	Classification of quantum dots. Several types and examples of quantum dots are given. (In alloyed quantum dots, the letter x represents the content ratio.)	11
3.1	Comparison of the production methods of silicon nanocrystals.	27
4.1	Comparison of doped nanowire production methods from several aspects	56

Chapter 1

Introduction

This work concerns design, fabrication and characterization of silicon nanocrystals doped nanowire array produced with iterative size reduction technique. Active material doped, well-structured nano-geometries have great importance for both basic research and applications [1, 2, 3, 4]. Furthermore, quantum dot (QD) doped/ decorated nanowires can be used for applications which need precise control, patterning and shaping without losing any functional properties of the embedded material or possibly enhancing them. Doped nanowire or nanofiber geometry can be utilized for increasing emission efficiencies, controlling emission direction, sensing applications or single photon extraction thanks to their one dimensional geometries [5, 6, 7]. Hence, simple and effective production methods could enhance the functionality of this type of structures without hindering any desired specifications. Thus, the motivation of this work is to develop a new method for production of such structures with using our iterative size reduction technique [8]. For this reason, starting from scratch to very end product, we designed and produced silicon nanocrystal embedded nanowires which can be used in potential research and applications. The produced nanowires present the applicability of the method and possess a high potential for utilization and improvement.

Quantum dots are luminescent nano structures having size of a few nanometers and emitting light at wavelengths in the range from ultraviolet (UV) to near

infrared (NIR). There are lots of quantum dot types which have different chemical and physical properties due to their chemical structures and surface modifications. Main application areas of QDs can be counted as bio-labeling, energy efficient lighting and display technologies [9, 10, 11, 12]. However, synthesis of most of the quantum dots is very dependent on experimental conditions (temperature, pressure *etc.*). Also, mass production of the dots is difficult due to high cost of production and critical experimental conditions. Furthermore, some types are hazardous for human health and should not be used in devices in contact with humans [13]. Hence, alternative structures to these types of dots gain value when the above mentioned aspect is considered. One of the mostly used alternatives is silicon quantum dots or silicon nanocrystals even though their quantum efficiencies are less than other types of quantum dots. There are lots of methods for synthesis of the nanocrystals like electrochemical etching, high temperature treatment with post etching [14, 15]. This work considers chemical routes are more compatible because of high product yield and simple production steps. In addition, they have much more stable luminescence to high temperature exposure. In summary, the above mentioned properties with the optimal choice for the synthesis make silicon nanocrystals the most suitable choice for production of luminescent nanowires with our iterative size reduction technique.

Nanowires are one of the most important simple geometries used in current research and application because of properties like high surface to volume ratios, light-guiding properties, higher roughness comparing to other planar geometries. Luminescent nanowires produced with several techniques has previously worked within a wide scope [6, 16, 17, 18]. Electrospinning, probe drawing, clean production techniques are some of the mostly used production techniques for the production of doped nanowires [19, 20, 21, 22, 23]. Here, with this work we present a new method for producing luminescent nanowires and nanowire arrays. The technique is superior to previously used methods from several aspects. First, the size of the wires may span whole range from hundreds of microns to a few nanometers whereas the length can be as long as hundreds of kilometers. Despite these outstanding properties, the final geometry is not complex unlike electrospun nanofibers which may have similar properties. Second, for applications

which need precise control, patterning and shaping, the fibers can be handled easily, which will be shown at Chapter 4. Third, the production simplicity is comparable to probe drawing techniques with above geometrical advantageous. With these superiorities, here we show that iterative size reduction technique is a versatile method to produce luminescent nanowires even though in the current level there are some challenges like concentration level of the active material which may be improved in future designs.

To sum up, the purpose of this thesis is dedicated to design and fabrication of silicon nanocrystal embedded nanowire array that can be used for light guiding, improving emission efficiency, sensing applications, fiber lasers and another fields of interests of research and technology. The flow of the work starts with a brief introduction. In Chapter 2, we will continue with quantum dots with their types and applications. Then, a review of active material embedded designs and fabrication of such structures will be considered. Chapter 3 will be dedicated to silicon nanocrystals. This chapter will give the details of synthesis and characterization of silicon nanocrystals and large area luminescent thin films. Fabrication and characterization of silicon nanocrystal doped nanowire array will be presented at Chapter 4. Finally, a more complete summary and future outlook will be given at Chapter 5.

Chapter 2

Quantum Dots and Embedded Designs

Quantum dots (QDs) are nano-sized, photoluminescent materials that radiate light at all the visible spectrum, near-infrared (NIR) and ultraviolet (UV). There are varieties of quantum dots in literature, especially ones with heavy metals are widely used in the current research and technologies. They usually consist of binary or ternary alloys. Furthermore, surface modifications, ligands and embedding than otherwise matrix structures are important aspects which can modify and enhance luminescence, solubility and stability properties of quantum dots. These modifications also enhance the usability of these QDs for possible applications and technologies. On the other hand, standalone nanoparticles are not very usable for quantum dot based devices and for potential applications, because of some lacks like luminescence quenching due to reasons like oxidation and photo-quenching. In this chapter, a relevant literature review of quantum dots and quantum dot embedded systems is given. It starts from a general consideration of quantum dots with their applications. Then, it is followed by a more specific topic of quantum dots embedded fibers. Finally, the production techniques are pondered.

2.1 Quantum Dots and Applications

Quantum Dots (QDs) are zero dimensional, nano-sized molecular particles that show properties both like crystals and single molecules. These properties are determined by the total effect of the atomic band structures and confinement effects in the crystals [24, 25, 26, 27]. A complete theory of the quantum dots can be given in book scale texts, which is beyond the scope of this work. Since the purpose of this thesis is not theory but applications of quantum dots, here we are contented with only introductory level information about the theory. However, the following argument is quite sufficient for basic understanding of the mechanism behind the photoluminescence from the quantum dots. For a more complete argument we can recommend the books by Pavese [27] and Harrison [25].

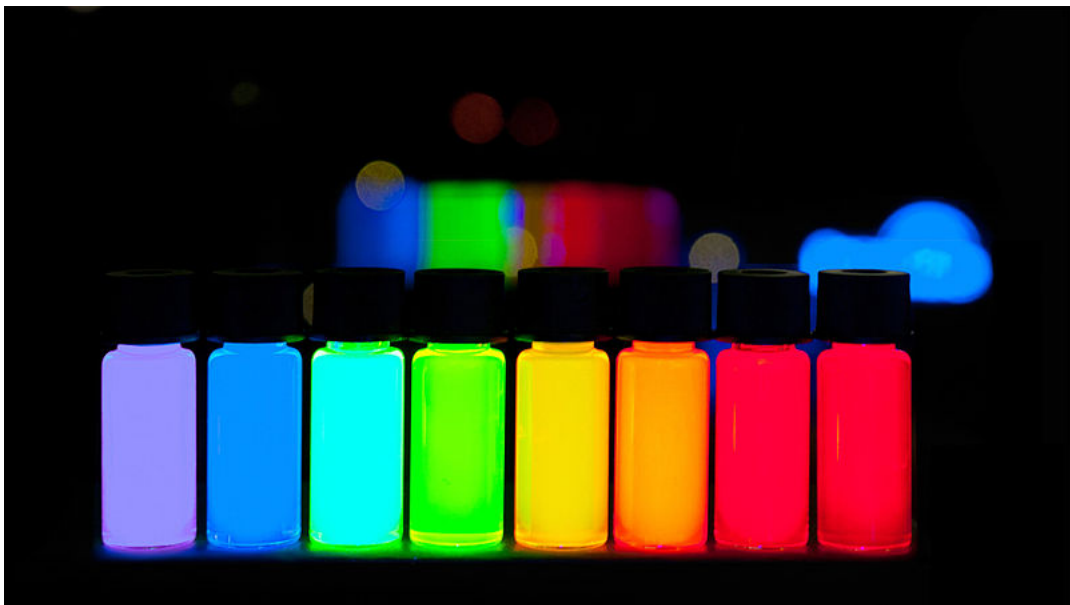


Figure 2.1: Quantum dots with vivid colours spanning from violet to deep red. (Adopted from Ref. 28).

The mechanism behind the photoluminescence (Figure 2.1) of QDs is a purely quantum mechanical phenomenon. Due to this reason, this property can only be observed in quantum regime, where the size of the system is comparable with the size of the effective particle which determines the system properties. For QDs, these particles are excitons which are built from an electron and a hole. Then, when the size of a crystal becomes smaller than its exciton-Bohr radius, the exciton will

be squeezed and it cause quantum confinement like a particle in a 3D quantum well. Hence, the energy levels will be determined by the size of the well which is size of the crystal in this case. When this confinement effect dominates, electrical and optical properties can also be determined by the size of the crystal. The fluorescence mechanism is quite simple such that when an excited electron comes to its ground state and with combining with a hole, they build an electron-hole pair (Figure 2.2). For the recombination, there are 3 possible scenarios; radiative, non-radiative and Auger recombination. In radiative case, the energy difference between initial and final states of electron is released as photons, which is the source of luminescence. The color of the luminescence depends on the energy levels of the corresponding electron and hole. The bound energy of this electron-hole pair determines the energy of the released photon hence the wavelength and the color.

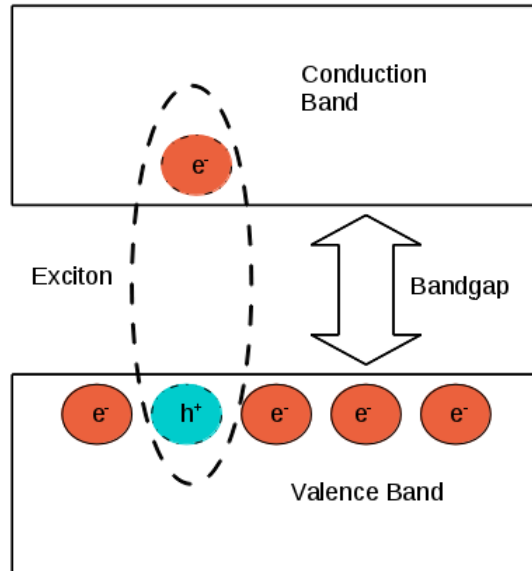


Figure 2.2: Exciton generation with the combination of an excited electron and a hole.

Strength of the confinement determines the energy levels of the structure. The confinement is said to be weak, when the crystal size is in the order of its exciton-Bohr radius and strong when the crystal size is smaller than the exciton-Bohr radius. The exciton-Bohr radius is given by,

$$a_b^* = \varepsilon_r \left(\frac{m}{\mu} \right) a_b,$$

where a_b is the Bohr radius, m is the mass, μ is the reduced mass and ε_r is the size dependent dielectric constant. The energy levels begins to split when the crystal size becomes smaller than this exciton-Bohr radius and leads to increment in band gap energy in the strong confinement regime (Figure 2.3). Hence, in the strong confinement regime which means that confinement energy is larger than band gap energy, the quantum confinement effect dominates and leads to splitting in energy levels and emission in various wavelengths. The confinement energy can be calculated with particle in a box model [25]. Then the total confinement energy is the sum of ground state energies of the electron and the hole. Hence, the confinement energy is written as,

$$E_{\text{confinement}} = \frac{\hbar^2 \pi^2}{2a^2} \left(\frac{1}{m_e} + \frac{1}{m_h} \right) = \frac{\hbar^2 \pi^2}{2\mu a^2},$$

where μ is the reduced mass, \hbar is Planck's constant and, m_e and m_h are the free electron and hole masses, respectively. In addition to confinement and band gap energies, there is one type of energy that is bound exciton energy, contributing to total energy of the structure. Since electron and hole are oppositely charged particles, there is a Coulomb interaction between these two particles. With the modification due to confinement effects, the Coulomb energy can be given as,

$$E_{\text{exciton}} = \frac{-\mu}{\varepsilon_r^2 m_e} R_y,$$

where μ, m_e, ε_r are as defined previously and R_y is the Rydberg's energy. Hence the total energy can be given by,

$$E_{\text{total}} = E_{\text{bandgap}} + E_{\text{confinement}} + E_{\text{exciton}}.$$

Thus, the above formula shows, in the confinement regime where confinement term dominates in the energy expression, electrical and optical properties

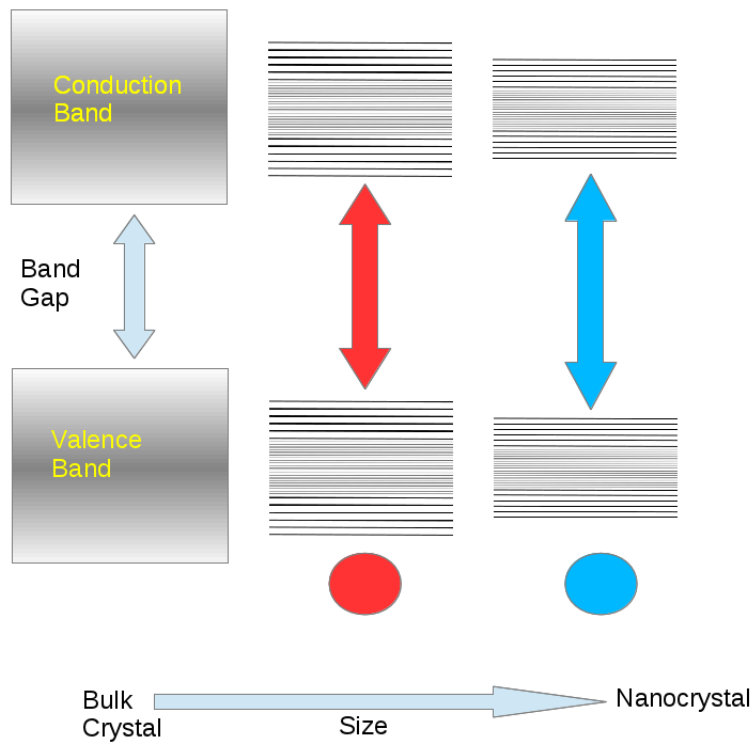


Figure 2.3: Size-energy band relationship in semiconductor quantum dots. Energy levels begin to split when the dimension of the nanocrystal quantum dot becomes to be on the order of its exciton-Bohr radius. Also, with decreasing size, the bandgap widens hence the luminescence shifts toward smaller wavelengths.

are determined by the confined states hence by the size of the crystal. When the crystal size dimension becomes smaller, the luminescence wavelength shifts toward to smaller wavelengths, which means increment in photon energy. For a quantum dot which gives emission at visible wavelengths, this mechanism is called as blue shift, and the reverse mechanism is called as red shift which corresponds to increment in crystal dimensions.

As discussed above, at the nanoscale dimension, materials show different properties than their bulk form, due to quantum effects. At this scale, conductivity, fluorescence, melting point, permeability and chemical characteristics are determined by the size of the particle. Because of its discrete energy levels, QDs behave likely to be single atoms or molecules. Thus, due to these properties, they can be called artificial atoms. Their emission spectrum is also very narrow, when there

is no external interaction. When there is an interaction, for example in a cluster of quantum dots, emission spectrum bandwidth broadens.

Up to this point, we only mentioned about the theory and general properties of the quantum dots. Indeed, each different type of quantum dot may show specific chemical and physical properties even though they emit photons at same wavelengths. On the contrary, same nanocrystals with different dimensions emit light at different wavelengths. Thus, the luminescence is dependent on both content and size. Hence, from now on, it will be more appropriate if we will continue with real examples of QDs. Also, classification of the types can be more easier and clear with these examples.

The first realization of the synthesis of the nanocrystal made by a Russian scientist A.Ekimov in 1980 [29]. In the following decades, lots of research about developing quantum dots have been promoted. At the current state, there are lots of different types of quantum dots are available commercially or as its production methods [30, 31, 32]. In the following, we will discuss quantum dot types which are the most frequently appeared in current research and technologies. Also, it will be suitable if we classify the quantum dots with respect to their composition and structure. Hence, we can study them in 3 main classes such that core type, core/shell type and alloyed quantum dots (Figure 2.4).

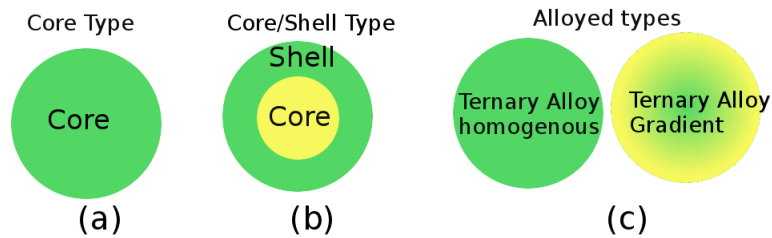


Figure 2.4: Schematic representations of quantum dot types. (a) Core types generally consist of two different elements which constitute crystal structure together. (b) Core/Shell type includes two different type of crystal structure built from different content crystals. (c) For alloyed quantum dots, ternary alloys can be homogenous distribution or a gradient through the volume.

Core type quantum dots are generally composed of two different elements

which belongs to groups III-V,II-VI and IV-VI in periodic table. In this category, we can give some examples from some of the mostly used ones like CdSe, InP, InAs, PbS and PbSe. The physical properties like photoluminescence and electroluminescence of core type quantum dots can be changed with changing nanocrystal size. Hence, a desired color can be simply obtained with adjusting crystal size. However, eventhough the process is simpler comparing to adjustment of the other types, the efficiency of core type dots generally less than other type dots. Like other types of dots, core type dots also suffer from photobleaching which may be due to time, physical or environmental effects. Also, silicon quantum dots and carbon dots can be counted in this category. Their quantum efficiencies are generally less than formerly mentioned quantum dots but these types of quantum dots constitutes no known health risk which is desirable while working with living organisms. Besides, they are much more durable to environmental effects. Abundance of the main material and easy fabrication methods make them more appealing. Table 2.1 lists of these types of quantum dots that are frequently used in research and applications are also given.

Quantum efficiency and stability of the quantum dots can be enhanced with introducing higher band gap semiconductor around the core type quantum dots [33]. The new structure is known as core/shell quantum dots. As explained above, If recombination of electron-hole pair occurs in radiative way, the quantum dots can emit photons. On the other hand, this recombination may occur in a non-radiative way such as with emitting phonons or with transferring kinetic energy to another electron. Non-radiative recombinations reduce the quantum efficiency of a quantum dot. In order to solve this problem, wider band gap semiconductors that are surrounding core type quantum dots can passivate non-radiative sites, hence increase stability and quantum efficiencies. In Table 2.1, several core/shell type quantum dots are listed.

In previously mentioned types of quantum dots, the color of the luminescence is determined by the crystal size. Thus, in order to get desired color, the size should be well-adjusted, which is not very practicable in most cases. However, in ternary alloyed quantum dots, with changing content ratio, the color can be tuned [34]. The alloyed quantum dots generally consists of three different elements

Table 2.1: Classification of quantum dots. Several types and examples of quantum dots are given. (In alloyed quantum dots, the letter x represents the content ratio.)

QD Type	Examples
CoreType	CdS, CdSe, CdTe, ZnS, ZnSe, ZnTe, HgS, HgSe, PbS, PbSe, PbTe, HgTe, MgS, MgSe, MgTe, GaAs, InP, InAs, InGaAs, IrGaAs, AlGaAs, Si-Nc, CD
Core/Shell Type	CdS/ZnSe, CdS/ZnS, CdSe/ZnS, CdSe/CdS, CdTe/ZnS, CdTe/CdS, PbSe/CdSe, CdSeTe/ZnS, CdHgTe/CdS
Alloyed	CdS_xTe_{1-x} , $CdSe_{1-x}S_x$, CdS_xSe_{1-x}

like in core type quantum dots. Yet, there is a difference between core/shell type and alloyed quantum dots. In core/shell type, the core and the shell are split from each other except the intersection points at the surface of the core. However, in alloyed quantum dots, composition of the elements can change through the whole structure, which can be also a gradient between the center and the surface. With these properties, they can be more durable and quantum efficient than their counterparts with more simpler color tuning. In Table 2.1, some of this type of quantum dots are listed.

Pure, bright and stable colors of quantum dots make them attractive for research and developing technologies. With QDs, high efficient lighting with low power consumption is possible [35, 38]. Also, QDs can be used for white color generation [39]. Because of their extremely small dimensions, the charge carriers can spend less time on them when carrying signals. Hence, it is possible to build faster electronic/optical devices, logic gates or transistors from QDs [40, 41]. In addition, there are other areas of research and applications where quantum dots are extensively used. They can be used in bio-imaging, bio-labeling or bio-targeting with making some modifications, even though some types are toxic [10, 36]. Also, quantum computing, QD LEDs and displays, QD solar cells and photosensors are some of the most appealing ones [37]. With an appropriate design it is possible to built lasers from quantum dots with special properties [42]. Some of the applications and designs related to quantum dots are shown in Figure 2.5 which includes a light emitting device (LED) design, quantum dot based solarcells and some uses of quantum dots as bioimaging and biolabeling. These are just a few examples of quantum dot embedded designs which show potential uses and application areas.

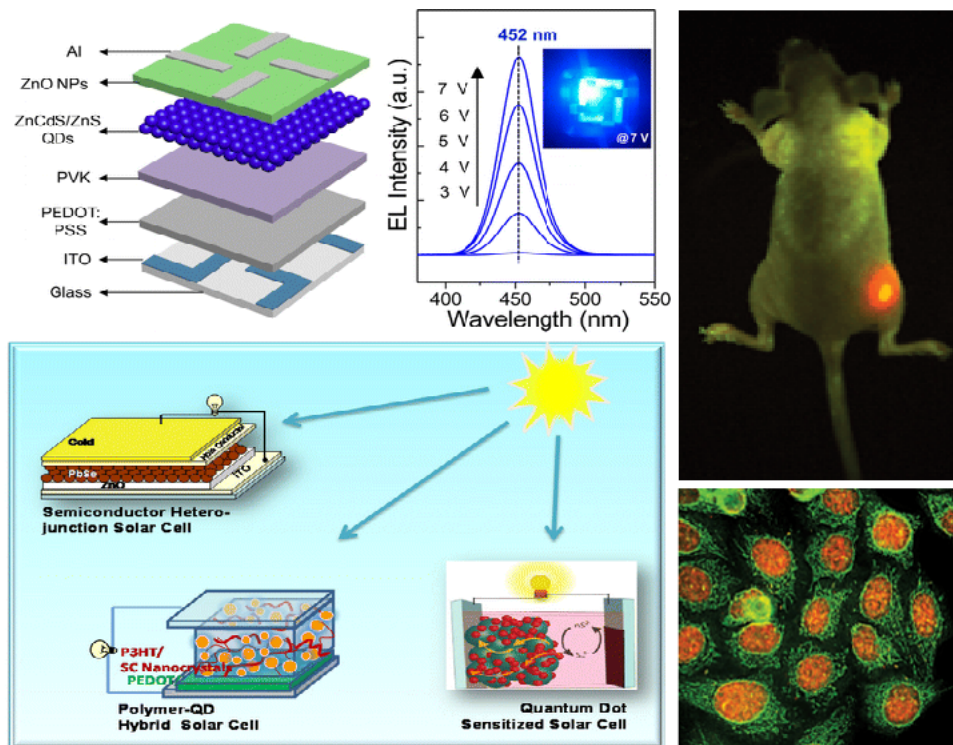


Figure 2.5: Some representative examples from applications of quantum dots. At upleft corner, a quantum dot LED is shown (Adopted from Ref.[35]). Quantum dots can be used for bio-labeling applications like in figure at upright corner or for bioimaging like in downright corner (Adopted from Ref. 36). At the downleft corner, schematic representations of several photovoltaic devices is shown. (Adopted from Ref. 37).

The research and application fields are still growing. In summary, quantum dots have lots of applications and a growing potential for new emerging research fields and applications which requires less energy, less time, on the other hand have pure, bright and stable colorization.

2.2 Active Material Embedded Luminescent Fibers

Decorating, doping or structuring fibers with active materials can increase usability limits of both fibers and active materials since they can combine properties of

both. The combination can give superior properties with control of both structure/geometry and content. As a special interest of this work, active material embedded luminescent fibers has great importance for both research and application. For light generation usual polymer and glass fibers are generally passive materials, except for conjugated polymer fibers. Besides, luminescent materials such as quantum dots give omnidirectional emission which is not desired in most cases. However, the combination of fiber geometry and quantum dot can give brighter luminescence in desired directions. In literature, directional emission, increasing emission efficiency, patterned or shaped lighting and single photon generation are some of the fields which realizes active material embedding to fibers which already have been worked extensively [6, 16, 17, 18]. Also, the interest to the concept still continues with a growing contributions to the field. In addition to the current state, new technologies and new research fields which cannot be realized before, may occur in near future with a proper engineering of the active materials and fibers. Among lots of active material embedded fiber designs, we can give some examples that can represent several concepts behind them. With analyzing these representative works we can get the principle behind the combination of active material with fibers. Thus, in the following, we give a brief review of such representative works.

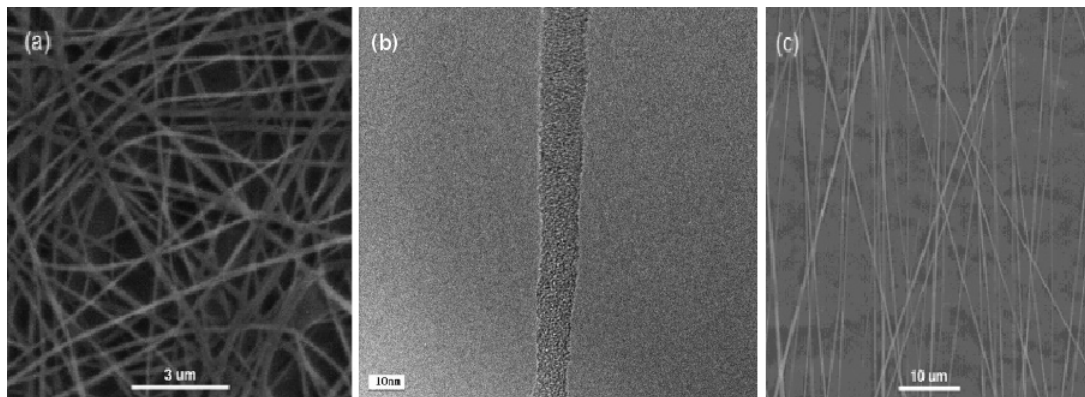


Figure 2.6: Some of the results gotten by Schlect *et al.* (a) SEM image of electrospun PLLA fibers (b) TEM micrograph of the electrospun PLLA fiber obtained via the frame collector approach (c) SEM images of oriented fibers. (Adopted from Ref. 5)

One dimensional light source embedded systems can be used as single photon

sources, directional emitters, light sources in integrated optics or photonic crystals with embedded light source. Also, linear array of quantum dots can show localization effects for light traveling. This phenomenon is similar to Anderson localization for electron transport [43, 44]. In order to realize the design and to observe subsequent results, quantum dot embedded nanofibers were fabricated with electrospinning by several researchers [5, 45, 46]. Schlect *et al.* used ZnSe quantum dots as dopant and polystyrene with polyactide as host polymer matrix [5]. With electrospinning the solution of mixture of dopant and host polymer, they achieved to produce fibers having diameter range between 10 nm and 100 nm (Figure 2.6.a,b). Also, with several different techniques they aligned the doped fiber in parallel fashion (Figure 2.6.c). However, they did not observe localization effects which was explained by packing of the fibers which makes the structure too dense and obstructing the effect. There are several similar other works which uses different fabrication techniques but realizes the same idea of luminescent fiber production [17, 18, 47]. As an example, quantum dot embedded PMMA micro-fibers were produced with thermal drawing [47]. In this work, the authors used the thermal elongation of the polymers in order to reduce the size of the doped structure having dimensions of several millimeters. In the previously mentioned works, authors used different techniques to fulfill the same goal of production of doped luminescent fibers, which demonstrates the importance of presenting new fabrication methods.

Fiber diameters less than dopant's radiation wavelengths can cause changes in physical properties of QDs like radiative decay rate. Tomzcak *et al.* showed that when the diameter of the fibers becomes less than the radiation wavelengths radiative decay rates increases for polymer fibers doped with luminescent dyes and particles [6]. The fibers produced with electrospinning with dopants core/shell CdSe/ZnS quantum dots and several dye molecules, discretely (Figure 2.7). They observed that the luminescence life time is not dependent on fiber diameter except when the diameter is below the luminescence wavelengths. This result explained by the change of electromagnetic boundary conditions which cause broadening in radiative decay rates.

Light emitting transistors and flexible light emitting switches can pave the

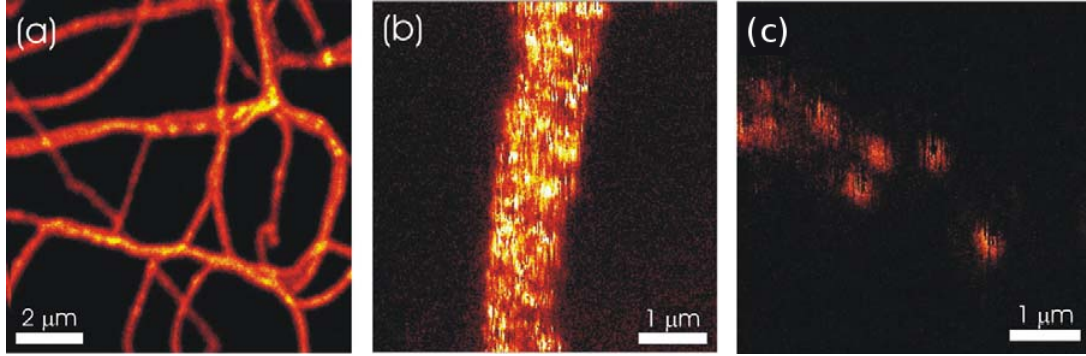


Figure 2.7: Some of the results gotten by Tomzcak *et al.* Scanning confocal fluorescence images of (a) DiIC1(5) dyes and (b) CdSe/ZnS quantum dots embedded in electrospun PEO (polyethylene oxide) fibers. The chromophores are distributed uniformly within and along the fibers, (c) QDs along PMMA fibers. Blinking behavior was observed which indicates that the fluorescence is coming from single light emitters. (Adopted from Ref. 6).

ways for optoelectronic technology which is very important for future developments in technology since the planar only electronic devices doesn't fulfill some requirements like flexibility. Tu *et al.* fabricated a polymer nanofiber light emitting field effect transistor (Figure 2.8.a,b) [41]. They fabricated the transistor with electrospinning luminescent polymers followed by metal contacting to aligned nanofibers. The electrical performances of the resulting transistor was comparable to or better than those of thin film transistors built from same polymer sets. Also, the gate voltage can be used to modulate photoluminescence. This design opens a way for one dimensional flexible optoelectronic devices which is highly demanding for current display technologies.

Electrically controlled designs are very important for current state of the art technologies and research, since it is simpler to control a system with a suitable electronic devices or with computers. Electrically controlled luminescent fibers can be the most realistic candidate for the elastic displays. Yang *et al.* fabricated an electrospun luminescent fibers which can be electrically controlled (Figure 2.8.c,d) [18]. Their design consists of three layer core/shell/shell structure. In the core of the fiber, there is electrically conducting liquid electrode. In the most outer shell, there is an ITO layer, which is electrically conductive and optically transparent at visible wavelengths. In between, these two electrodes there is an

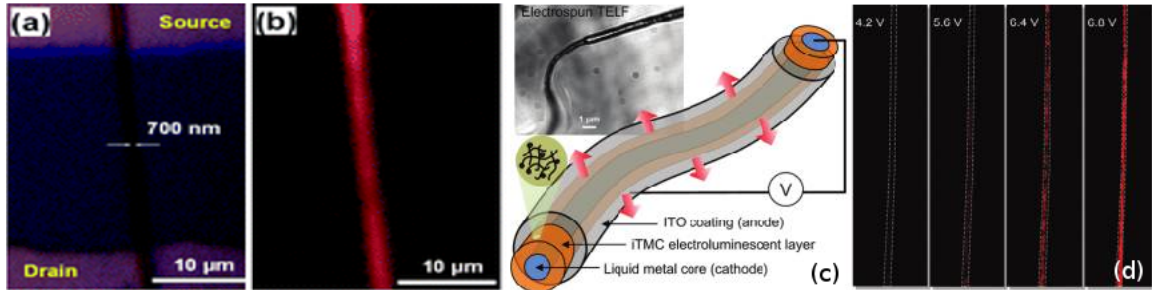


Figure 2.8: Light emitting fiber FET and electroluminescent fiber designs. (a) Bright field and (b) fluorescence micrographs of a single light-emitting fiber FET built by Tu *et al.* (Adopted from Ref. 41) (c) Schematic representation of light emitting fiber and (d) resulting luminescence from this design. (Adopted from Ref. 18)

active region which emits light when electrically pumped. As they claimed, this design has potential to be used in several areas like imaging, sensing, microscopy or flexible displays.

Another way to build luminescent fibers is to produce light guiding structures that modulate incoming light and gives desired color at desired direction. With the use of this idea, it is possible to build flexible displays with a suitable patterning of the fibers. Yu *et al.* fabricated such polymer fibers with direct drawing from a polymer melt [48]. Subsequently, they patterned the structure with micro-manipulators in a crossed-rectangular matrix geometry and with the use of correct launching directions, luminescent points at the matrix were held (Figure 2.9.A). With similar geometries, they got several colored pixels which are the building block of a display. With this design, they open a way to build multi-colored displays without using color filters. The color can be adjusted with only editing power ratios launched in the fibers. Similarly, it is reported that waveguiding excitation into luminescent fibers can increase excitation efficiency [16]. The authors only showed the concept for dye doped fibers but it may work similar for other QD doped or conjugated polymer fibers, as well. As they proposed, with appropriate design the fibers with waveguiding excitation can be used as bio-sensor thanks to the change in coupling ratios when an analyte interacts with the system. Then the ratio will depend on analyte concentration hence will sense the desired molecules.

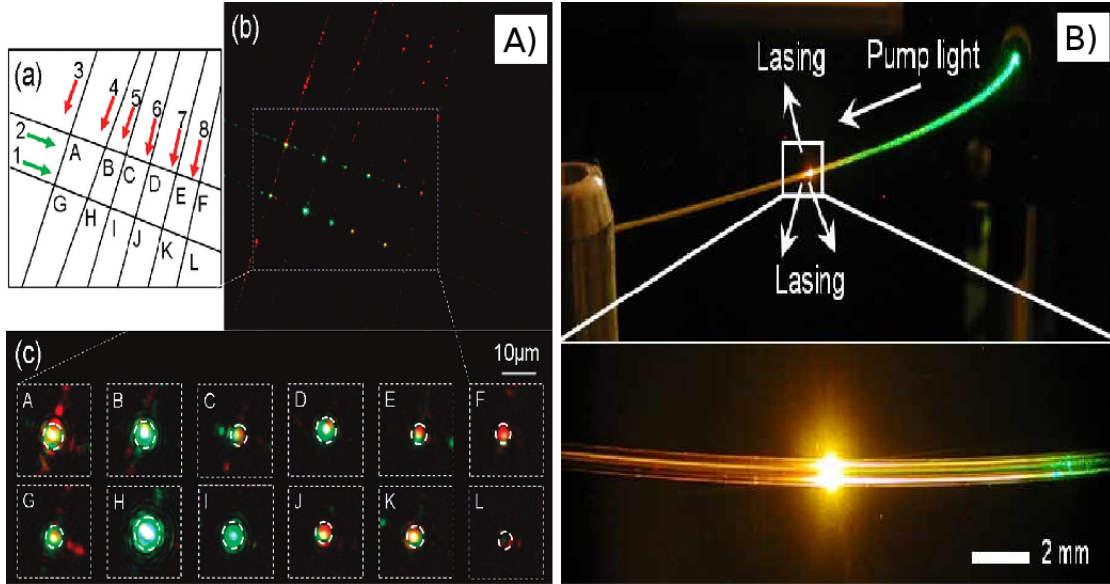


Figure 2.9: All optical display designs and surface emitting fiber laser. A) Schematics of the array structure and resulting color mixing and magnified images of luminescent points. (Adopted from Ref. 48). B) A photograph of an R590-doped fiber showing the pump (532 nm, green) and the lasing at 576 nm (orange). (Adopted from Ref. 22).

Active material embedded luminescent fibers can be used to built lasers. In order to get lasing it is well known that one needs a light generation medium and a resonator structure. It is reported that with using dye doped microfibers with surrounding Bragg like structure, it is possible to build surface emitting fiber lasers (Figure 2.9.B) [22]. Contrary to the most general fiber designs, their design emits light from its surface rather than fiber axis. This design uses one dimensional photonic crystal structure in order to control light emission direction from dye doped luminescent core. With using different colored dyes, they achieved to get fibers lasing at different wavelengths. They proposed that their design can be used in in-vitro imaging, flexible displays or in optical sensing.

In this section, we gave several representative examples that show importance of the active material embedded luminescent fibers or nanowires. In addition to given examples, there are lots of similar other works. However, we were contented with giving a few examples since it will not be practicable in other case. The examples were sufficient for getting general idea behind active material embedded

design. For a more deeper understanding, one can look up for other similar designs.

2.3 Fabrication Techniques for Producing Nanostructures

For the fabrication of active material embedded designs lots of techniques have been built and developed. Non-complexity, reproducibility and low cost producibility are important concepts of the fabrication. Also, the process should not be harmful for desired properties. Since we are dealing with fiber geometry, we only explained a few of the production methods among lots of fabrication methods of nanostructured geometries [19, 20, 21, 22, 23]. Here, we give explanations of some of the most relevant ones to our work. When measuring the success of a fabrication method, one should consider the requirements and desired properties of the final product. Each production technique has advantageous and disadvantageous sides from several aspects. However, several general criterion are important for all designs, and for the comparison of the techniques, we can use them. As we mentioned before, for the production to be highly applicable, it should be non complex, reproducible and low cost affordable. In addition, for the end product, we can count several desired properties like, uniformity, high yield production rate, patternable and easy size controlled geometries. From this point of view, we can compare and find the most suitable one for the design under consideration. For the optimal choice, the properties mentioned above should be well-known. For this reason, in the following, several doped fiber production techniques are explained with their positive and negative attributes.

Electrospinning

Ionic or partially charged molecules or larger charged compounds can be accelerated between two oppositely charged electrodes. With using this idea, from a chemical mixture it is possible to fabricate fibers with simultaneously charging small amount of mixture in a needle of syringe and applying an electric field with

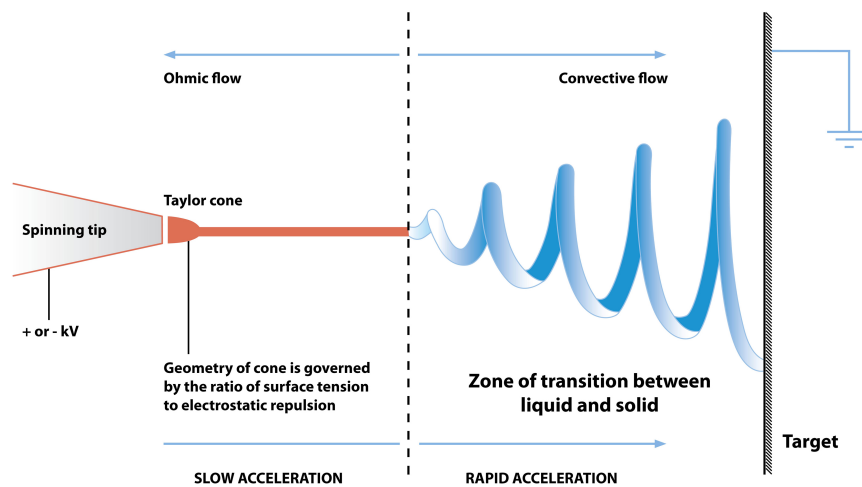


Figure 2.10: Schematic diagram of electrospinning process. With applying a high voltage difference, molecules in the solution both polarized and subsequently accelerated toward the target. With a continuous supply of both solution and electric field, fibers can be constructed on the target.

oppositely charged electrode at a distance. Since the needle and the electrode are oppositely charged, the mixture on tip of the needle will be accelerated towards the electrode. With a fine adjustment, this mechanism can be used to produce continuous flux between the needle and the oppositely charged electrode. This method is known as electrospinning (Figure 2.10). Also, with a proper choice of the size for the tip and the needle and with a suitable applied voltage, a few nanometer sized fibers can be held with this method, in a very simple way. The critical conditions for the electrospinning are the compound preparation and finding the most appropriate drawing parameters for the desired result. The production yield of this method is very high. However, resulting geometry is generally very complex. Even though, there are several methods for aligning resulting fibers, electrospinning falls behind its alternative drawing techniques from this aspect. However, electrospinning is one of the most simplest method for production of doped nanofibers.

Probe Drawing

Starting from a mixture of host matrix solution and dopant molecules, it is possible to fabricate fibers with directly drawing fibers with injecting and drawing

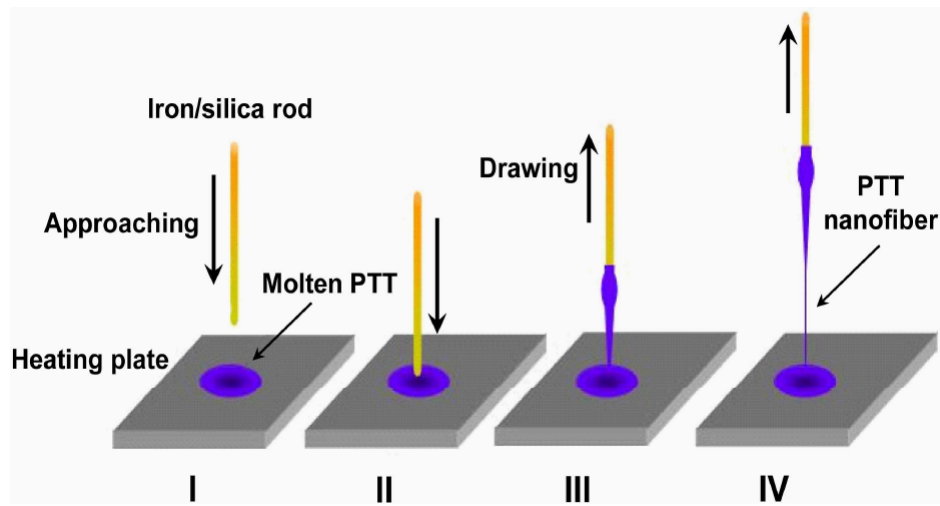


Figure 2.11: Schematic illustration of nanofibers fabrication by direct drawing process from molten polytrimethylene terephthalate (PTT). I, An iron or silica rod is approaching the molten PTT. II, The rod end is immersed into the molten PTT. III, The rod conglutinated PTT is being drawn out. IV, A PTT nanofiber is formed. (Reprinted from Ref. 21)

probes to and from the mixture [16]. When the injected probe is drawn to a template from solution with certain velocity, depending on the viscosity of the solution and the thickness of the probe, structured fibers will be formed on the template. The diameter of the fiber is determined by the viscosity, drawing velocity and probe thickness. This method is simple alternative to electrospinning but the product yield is much more smaller. However, the resulting product could be aligned easier comparing to electrospun fibers and the geometry is not complex, that is simply one free standing active material embedded fiber. A parallel method to solution probe drawing can be done with drawing from a melt [21]. A melt of desired content can be prepared with applying heat to mixture of materials under consideration. Subsequently, within this liquid phase, very similar to the above probe drawing, fibers can be produced with injecting and drawing probes to/from the melt (Figure 2.11). Again, the critical parameters are the same that are viscosity, drawing speed and probe thickness. The resulting fibers has similar properties with solution probe drawn fibers. In summary, probe drawing constitutes a solution for production of structured or doped fiber within a very simple way but with some lacks like low product yield.

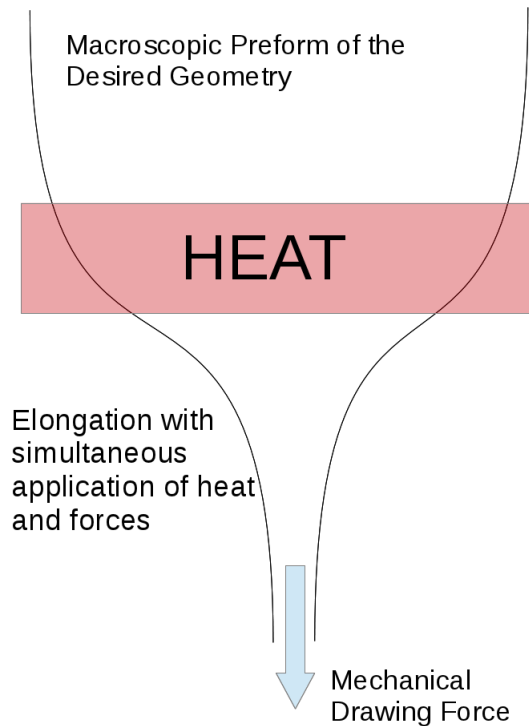


Figure 2.12: Schematic illustration of thermal drawing process. Size of the materials showing glass properties can be reduced with simultaneous application of heat and force. This results to size reduction in perpendicular directions to drawing forces while increment in parallel directions.

Thermal Drawing

Materials that shows glass properties can be elongated with applying heat. The basic mechanism behind the thermal drawing is to reduce the size with elongating the macroscopically large preform [49, 50]. During the elongation, a dimension perpendicular to elongation axis reduces whereas a parallel dimension increases. Also, shape and structure are generally preserved but overall sizes become smaller except parallel ones as shown in Figure 2.12. Some polymers like polycarbonate (PC), polysulfone (PSU), polymethylmethacrylate (PMMA) can be used in thermal drawing with lower temperatures comparing to inorganic glasses like silicon based glasses. Thermal drawing is a simple technique but drawing conditions should be well adjusted in order to get desired end product. Heat distribution, drawing and feed speeds are crucial parameters of the thermal

drawing. Also, specific material properties are effective during drawing. With thermal drawing kilometers long, uniform fibers can be produced. The initial and the final sizes depend on the size reduction ratio of the drawing process under consideration. However, initial preform dimensions generally are chosen to be a few centimeters and the final dimensions can be as much as a few millimeters and as little as a few microns. Hence, with this type of drawing, starting from a suitable preform it is possible to fabricate structured fibers [51]. Also, since initial designs have macro dimensions, it is simple to fabricate complex geometries like photonic crystal structures with this method [22, 52]. Modifications can enhance the overall desired properties of the fibers. In summary, thermal drawing is simple but effective method for producing structured and complex fiber geometries. The theoretical background will be handled with more detailed explanation in Chapter 4.

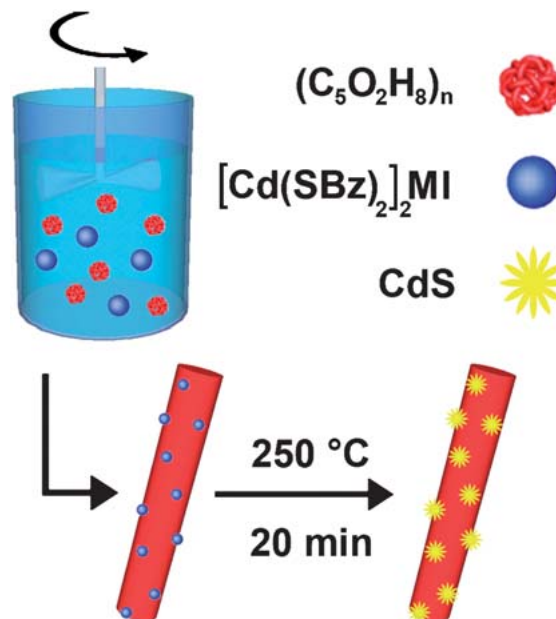


Figure 2.13: In-situ generation of CdS quantum dots in electrospun PMMA fibers. Quantum dots synthesised after production of the fibers with applying an external triggering treatment. (Adopted from Ref. 53)

In-situ Dopant Generation and Decorated Fibers

As an alternative approach, fibers can be decorated with active materials after production of the fibers [23]. This can be realized with simply putting

active materials on the fibers or with in-situ generation of the desired molecules from precursors after production of the fibers [19]. With former design, there is not much work to do and extra gain from the design, such that this decoration is not physically stable and since it is at outside of the fiber, it does not fully take the advantage of the fiber geometry. However, latter one has an important advantage and superiority to alternative methods. Most of the above mentioned methods harm the physical and chemical properties of the dopant up to some degree, even it is very small in most cases. In this procedure, since the desired dopant structure is formed after drawing, the preparation and drawing processes does not harm the dopant. In other words, not the final form of the dopant but its precursor is embedded to the fiber and after drawing with suitable treatment the precursors can turn into the desired dopant molecules, resulting to desired doped fibers (Figure 2.13).

Iterative Thermal Drawing

Iterative thermal drawing paves a new way for producing nanostructure doped polymer fibers [8]. With this production method we introduce an original doping produce which has superior properties in several aspects to its counterparts. Since this work based on the iterative thermal drawing, the detailed explanation of this technique and the comparison with other methods are presented in Chapter 4.

Chapter 3

Synthesis and Characterization of Silicon Quantum Dots and Silicon Nanocrystal Doped Polymer Films

Silicon quantum dots or, equally phrased, silicon nanocrystals (Si-Nc) are nanocrystalline structures that shows photoluminescence property at visible range, which are not shown by bulk silicon crystals [54]. With their luminescence property they constitute an alternative for other types of quantum dots eventhough their efficiency is far below its counterparts. In addition, for large scale applications and potential technologies, experimental simplicity, non-toxicity and low-cost producibility are important aspects. The synthesis of Si-Nc's is easier to conduct comparing to heavy metal QDs which is harder due to critical experimental conditions (pressure, temperature *etc.*) and resultant product of which is toxic [13, 55]. Thus, although current efficiency of silicon nanocrystals is far below heavy metal QDs, the above mentioned aspects makes silicon nanocrystals more attractive for lots of research and for our current design. In this section, a detailed explanation of the silicon nanocrystals, their synthesis, end-product characterization and silicon nanocrystal doped polymer films are given.

3.1 Silicon Nanocrystals

Silicon is most effective element in the current technological level of humankind, because of its abundance and its physical and electronic properties. However, since bulk crystalline form of silicon has indirect bandgap, they cannot be used in applications which is based on light generation. Yet, there is a remedy for this lack. Reducing the total crystal size to dimensions which are comparable with its exciton-Bohr radius can make them generate light through exciting it with an appropriate source. When this happens, the structure begins to show some new properties like photoluminescence. Although there are lots of theories in literature about the source of this luminescence, it is not crystal clear at the current level. As mentioned before, silicon nanocrystals are nanosized particles that show photoluminescent properties. Even though quantum efficiency of this type of nanocrystals are far less than other types of quantum dots, they are still attractive for research and technologies due to their low-cost, comparatively simpler production methods, high durability at both normal and extreme conditions, and non-toxicity to organisms. Because of these reasons, the interest to the Si-Ncs are growing since the first observation of luminescent Si-Ncs in porous silicon at 1990 [56]. Here, in the following sections, we give an explanation of the nanocrystal structure, theories about source of the luminescence, production methods and applications of silicon nanocrystals.

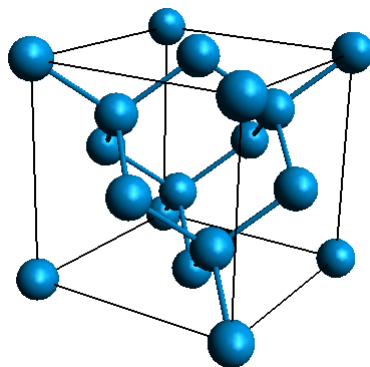


Figure 3.1: Diamond lattice of silicon nanocrystal. Thermal annealing of the HSQ molecular precursor leads to formation of nanocrystalline silicon that has diamond lattice. The final size of the crystal is dependent on experimental conditions.

The related crystalline form of the silicon nanocrystals is a diamond lattice (Figure 3.1) [15]. They are generally held in the form that is surrounded with a glass matrix or other passivation layers like hydrogen. Size and interactions between surrounding layers determines the luminescent properties [54, 57]. Also, depending on the fabrication method there can be several silicon nanocrystals in the same glass matrix. In addition, overall structure is very dependent on the synthesis method such that they can be on a planar surface such as wafers or can be dispersed in a solution. The synthesis method also determines the size distribution. The size distribution is an important concept for silicon nanocrystals since the luminescence spectrum broadens when size distribution is broad.

Even though there are lots of explanations about the source of the luminescence from silicon nanocrystals, the actual mechanism is not clear yet [54]. In the bulk form, silicon crystal has indirect band gap, thus transitions do not result as radiation in visible wavelengths. However, when the overall crystal size reduces down to a few nanometers, quantum effects dominate in energy bands [57]. The band gap becomes direct and the transitions can result as light emission. However, the dominance is not clear for the responsible states for the luminescence. It is thought to be both surface states and confined states that are responsible for luminescence. The effect of each is generally determined by size and surface passivations. Generally, when the molecular structure is kept same, increasing the size of the crystal shifts the luminescence to longer wavelengths. Also, the converse is also true that decreasing size decreases the luminescence wavelengths which is called blue shift. The type of the passivation is also important aspect for the energy bands hence for the luminescence color. Depending on the passivation elements, the emission color may drastically change [14, 58]. Hydrogen and oxygen are the most important ones. The emission wavelengths can increase with the change of passivation layer from hydrogen to oxygen [14]. The observations show both the size and the passivation layer are responsible for determination of the emission color.

For the synthesis of silicon nanocrystals, there are several methods including Si ion implantation, chemical vapor deposition, magnetron sputtering, colloidal synthesis, electron beam evaporation and e-beam lithography combined

Table 3.1: Comparison of the production methods of silicon nanocrystals.

Property\Method	Chemical	Wafer Based	Clean Production
Complexity	weak	moderate	excellent
Product Yield	excellent	weak	weak
Uniformity	weak	moderate	excellent
Example	High temperature treatment with post etching	Electrochemical etching of Si-wafers	Chemical Vapor Deposition(CVD)

with reactive-ion etching [27, 59]. Also, electrochemical etching of Si wafers and high temperature treatment are several alternative methods that are used to produce Si-Nc [14, 15]. Each method has advantageous and disadvantageous sides for getting desired properties. A comparison of the methods is given in Table 3.1. With these methods, crystal sizes around 5 nm can be synthesized. Preparation conditions and fabrication method determine the resulting physical properties. Besides, as a common property high potential barrier encapsulation can be seen in all types, in a form of air or passivation element layer. Due to type and size of this encapsulation layer, the color of the nanocrystal luminescence can be changed. As an example, hydrogen passivation gives smaller wavelengths comparing to oxygen passivated nanocrystal that has same crystal dimensions [14]. The properties of the passivation layer depend on the preparation and production conditions and type of the synthesis. In summary, the final chemical and physical properties of the silicon nanocrystal are determined by the method and the conditions during production processes. Furthermore, the surface can be further modified to enhance properties like solubility or to functionalize the surface for imaging or labeling.

Silicon nanocrystals have been used in various research areas and applications. However, since we cannot review all of them here, we focused on some representative applications which can give a general but helpful perspective to understand the potential of Si-Ncs. Exploiting the luminescence of the silicon nanocrystal, it is possible to build light emitting devices (LEDs) from silicon nanocrystals (Figure 3.2.a) [60]. With a proper engineering of the material and the device geometry electroluminescence from nanocrystals can be controlled and

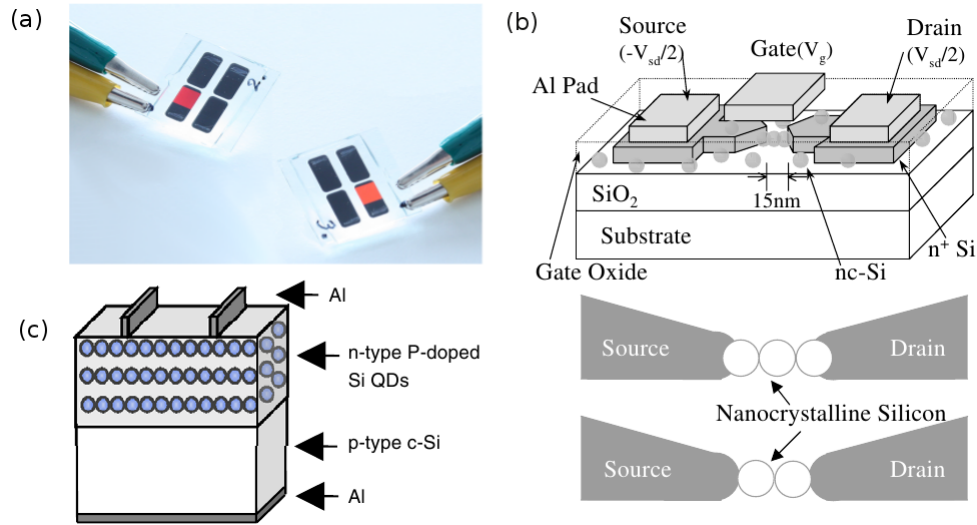


Figure 3.2: (a) Light emitting devices (LEDs) built from silicon nanocrystal (Adopted from Ref. 60). (b) Silicon nanocrystal utilized photovoltaic cell (Adopted from Ref. 61). (c) Silicon nanocrystal utilized field effect transistor (FET). (Adopted from Ref. 62).

utilized. Even though, quantum efficiencies of silicon nanocrystal are lower than its counterpart quantum dots, with doping rare earth metals or other dopants like phosphor, it can be increased [63, 64]. Also, the abundance and the low cost producibility make it more useful when developing a device like LEDs. As a second application of silicon nanocrystals, we can give electronic devices like field effect transistors and non-volatile memories [62, 65]. Because of its unique properties, it enables building single electron transistor from silicon nanocrystals which decreases energy requirements and heat generation while increasing switching speeds (Figure 3.2.b). Also, they can be used to store data with utilizing its charge storage capability as in non-volatile memories. Another exciting application area of silicon nanocrystals is photovoltaic cells. Since the absorption and the electronic structure of the silicon nanocrystal can be adjusted with changing the size and the passivation layer, it is possible to build a cell that contains crystals that absorbs light at several different bands which will increase the overall efficiency of the cell (Figure 3.2.c) [61]. In summary, silicon nanocrystals have high potential for developing new technologies and for improving already realized designs, and increasing interest to the subject can bring it to reality much sooner.

3.2 Synthesis and Characterization of Silicon Nanocrystals

As mentioned before, for the synthesis and functionalization of Si-nanocrystals, wide varieties of methods have been developed [14, 15, 66]. Among many of the synthesis methods, high temperature annealing of precursor material followed by etching treatment was the most suitable one for our design, since it can be done with experimental ease. It gives high amount of end product and it is highly repeatable even though resulting size distribution was not very uniform [15]. Also, in order to make size distribution more uniform, there are several methods available in literature [67, 68]. However, extra experimental procedures increases complexity of the design which is in conflict with the soul of this works. Hence, here we tried to set best experimental conditions for getting the most uniform size distribution for the nanocrystals. Since our aim was to prove the concept, the size distribution of our nanocrystal was sufficiently uniform to realize the design. Further developments and improvements or replacements will be done for future designs when needed.

In brief, the process was started from HydrogenSilsesQuioxane (HSQ) molecular precursor with extraction of the solvent in which HSQ is commercially available. This process yields a white powder and after high temperature annealing crystallization occurs resulting to silicon micro/nano-crystals embedded in a glass matrix. However, the size of the crystals should be reduced in order to get visible light emission when excited. Hence, with post etching treatment with Hydrogen Fluorine (HF) acid solution gives the desired result with different time requirements for different colors. Finally, the luminescent crystals, extracted from solution with pentane using phase separation where silicon nanocrystals choose to suspend in pentane.

In above paragraph, summary of the procedure was given. Here a more detailed view of the whole synthesis step may be given with separating each production step. Since several methods have been developed for the synthesis of the silicon nanocrystals, it may be more appropriate to start the steps from the

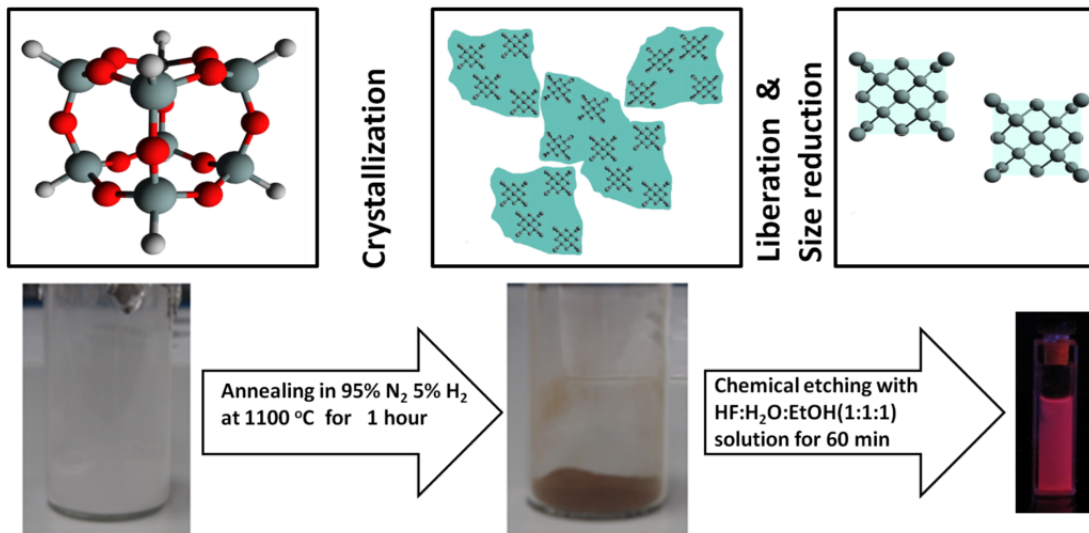


Figure 3.3: Synthesis of silicon nanocrystals. The synthesis starts with annealing of the HSQ precursor, following with grinding for further size reduction and uniform size distribution and finally with chemical etching, luminescent nanocrystals are held. Etching time determines the resulting coloration. Also, initial size distribution is effective for determination of etching time requirements.

choice of the route for the synthesis. Yet, it was only a consideration but not an experimental engagement, thus we left it as a preprocess item. As we mentioned before, the consideration was that for high amount of final product, chemical routes take the advantages although the final size distribution is not uniform as other methods such as electrochemical etching of Si wafers. High output rate and experimental simplicity of the purely chemical methods make chemical routes two step ahead of the other processes for a high concentration doping processes like ours. Hence, silicon nanocrystals were synthesized by a chemical method in 4 steps as follows which is parallel to the procedure in Ref. 15,

- 1. Solvent extraction from commercial HSQ precursor.** Commercial form of HSQ precursor (Dowcorning Corp.) is available in toluene solution. In order to be used in our process, solvent should be removed. After removal of the solvent, white HSQ powder was obtained.

- 2. High temperature thermal annealing at inert atmosphere.** white HSQ powder placed in quartz bath was annealed at 1100 °C at high temperature

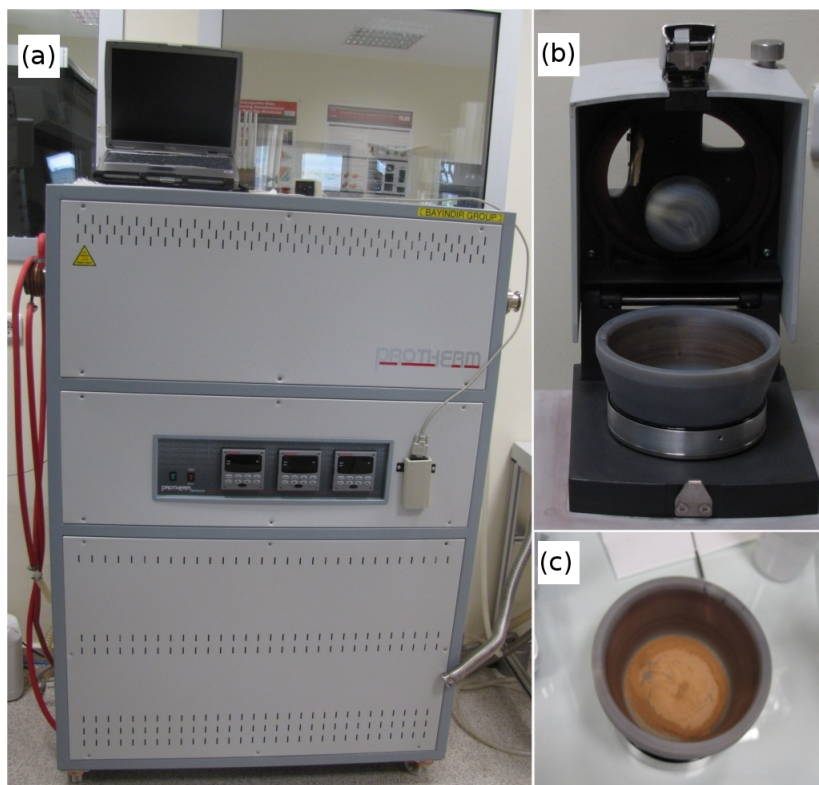


Figure 3.4: (a) Computer controlled high temperature furnace used for annealing the precursor molecules of silicon nanocrystals. (b) Auto-mortar used for grinding resulting silicon nanocrystal powder after high temperature annealing and (c) the powder after treatment.

furnace (Figure 3.4.a) with supplying H_2/Ar (4%, 96%) atmosphere at a constant regulation rate. The temperature was gradually increased from room temperature to $1100\text{ }^\circ\text{C}$ with $20\text{ }^\circ\text{C}/\text{min}$. After an 1 hour treatment, the system cooled down to room temperature. After this step white HSQ powder turned into brown/black Si/SiO_2 crystal structure.

3. Grinding and shaking of resulting powder from thermal treatment. In order to get fine powder of Si nanocrystals, resulting Si/SiO_2 has been ground in auto-mortar with pestle about 10 min (Figure 3.4.b and c). After grinding, the powder with 1 micron average particle size, dispersed in distilled water and after addition of glass beads, it was placed in a shaker. With treating in this way for two days, particle sizes decreased to hundreds of nanometers with average of 450 nm.

4. Chemical etching with HF solution with corresponding time requirement in order to get desired color. 1.2 g of the resulting powder was etched in teflon beaker with a solution of HF/H₂O/Ethanol(13.2:13.2:13.2 mL) mixture. The resulting color is determined by the etching time. For our initial particle size distributions 60 min etching gave bright red/pink color under UV irradiation. After etching 60 min, Si nanocrystals extracted from HF solution using pentane with using phase separation (Figure 3.3).

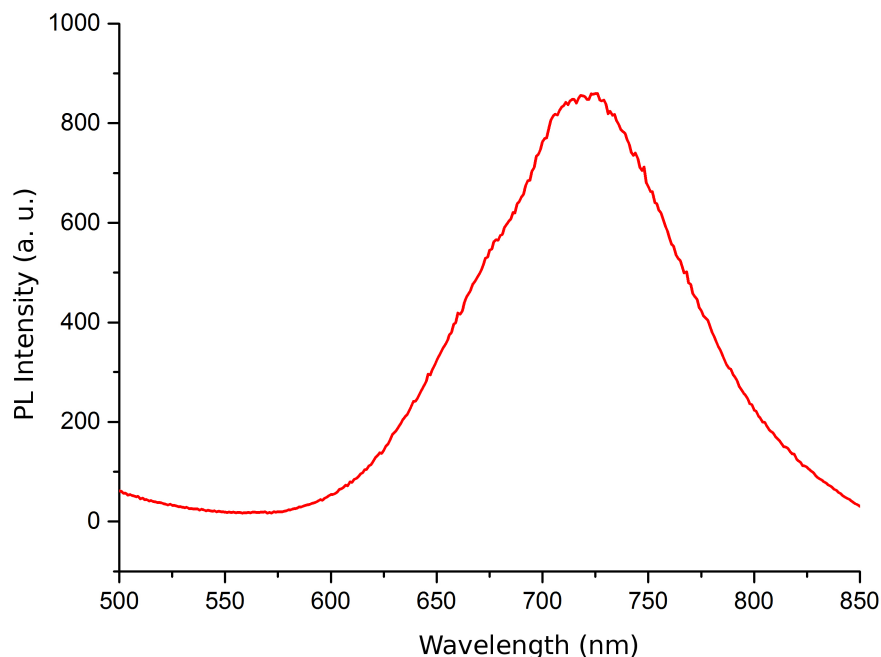


Figure 3.5: Measured PL intensity of silicon nanocrystals dispersed in pentane. The peak corresponds to red color. Also, the shape of the curve is measure of relative size distribution. In other words, there are nanocrystals emitting other colors rather than red but their number is small comparing to red emitting nanocrystals.

The characterization of the produced silicon nanocrystals was done with measuring the photoluminescence intensity of the products. The measurement were conducted with Varian Cary 500 Eclipse with exciting the solution sample with 325 nm light which is produced with internal light source. Figure 3.5 shows the corresponding measurement. In the graph, the bell shaped curve is centered at

around 710 nm, which agrees with the apparent color. The tails of the shape around the peak are a measure of the nanocrystal size distribution which means that there are lots of nanocrystals having different dimensions, emit photons from wavelengths ranging from approximately 550 nm to 850 nm. However, the number of the nanocrystals emitting around 710 nm is the largest one resulting to a peak at that number and the solution seems red because of this dominance. The results shows that the synthesized nanocrystals shows characteristic color, as expected from procedure [15]. The behavior of the nanocrystals are determined by initial crystal size distributions and etching time. In other words, for larger initial sizes, one should wait longer in order to get same color. HRTEM image of Si-Ncs are shown in Figure 3.6.a, which shows the crystal structure and the corresponding electron diffraction pattern is shown in Figure 3.6.b. Our results support the mechanism behind the luminescent behavior since decreasing crystal size with HF causes to a shift towards the smaller wavelengths.

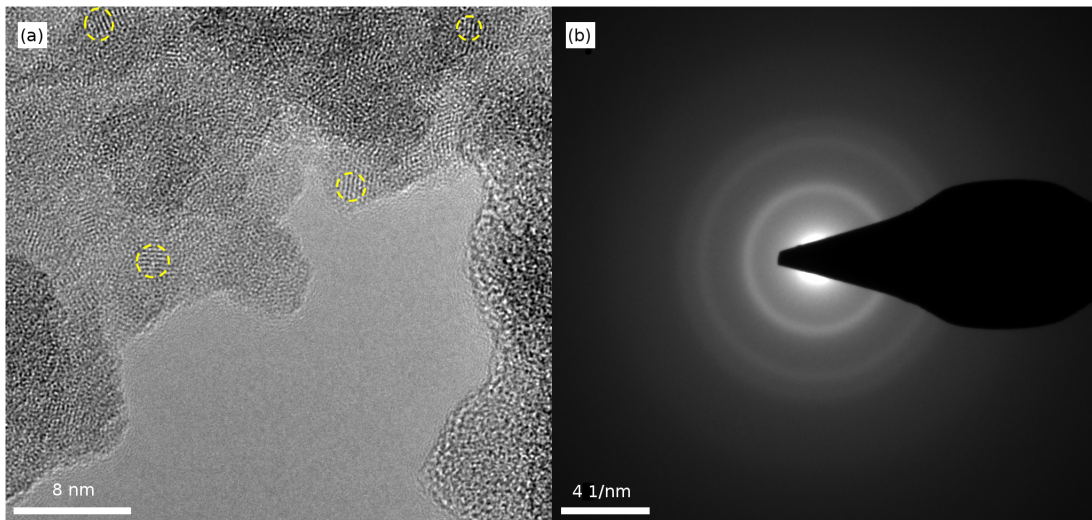


Figure 3.6: (a) High Resolution TEM image of silicon nanocrystals in surrounding SiO_2 matrix. Crystal sites can be seen in yellow circles. The regular patterns corresponds to crystalline silicon whereas irregular patterns belongs to amorphous glass matrix. (b) Corresponding electron diffraction pattern of crystalline silicon. The rings corresponds to distances between lattice planes.

A second characterization related to the resulting Si-Ncs was measuring the temperature dependent photoluminescence of the synthesized silicon nanocrystals. The data will also be used for comparison with the nanocrystals embedded

in polymer film, which will be discussed in the next section. The experiment was conducted with nanocrystal coated quartz wafer. At the beginning a quartz wafer coated with silicon nanocrystals which were suspended in pentane, with dip-coating method. After this coating, successive PL measurements were made after holding the sample at different temperatures with a step of 25 °C for the same duration of 20 min. This experiment was repeated for several samples. The behavior was not exactly the same but its tendency was very similar. Figure 3.7 shows the results of the experiment. By increasing temperature, the luminescence intensity decreases and blue shifts [69]. Oxidation and reduced size of the crystals is probably responsible for this effect. Here, our results agree with the expected behavior such that the luminescence decreases and shifts towards smaller wavelengths due to increasing temperature, which caused by the crystal size reduction. Another result which can be taken from this experiment is that even such high temperature as much as 225 °C, there is still luminescence. In the next section, we will show that embedding nanocrystals to a polymer matrix increases this durability which is a more desired result. In summary, silicon nanocrystal were successfully synthesized and characterized. The characterization and the measurements shows the suitability of these nanocrystals in our doped fiber design.

3.3 Large-Area Silicon Nanocrystal Doped Thin Films

Following to the synthesis of the nanocrystal, the next consideration was the selection of the host polymer and the development of a new doping method suitable to iterative size reduction method for the production of the doped fibers. First, the host matrix was determined. After investigating several types of polymers, polycarbonate thin films were chosen to be host matrix. The refractive index of the polycarbonate which is around 1.58 at corresponding wavelengths and glass transition temperature which is 147 °C are the most suitable one for our design among the available polymers. The importance of the refractive index comes from

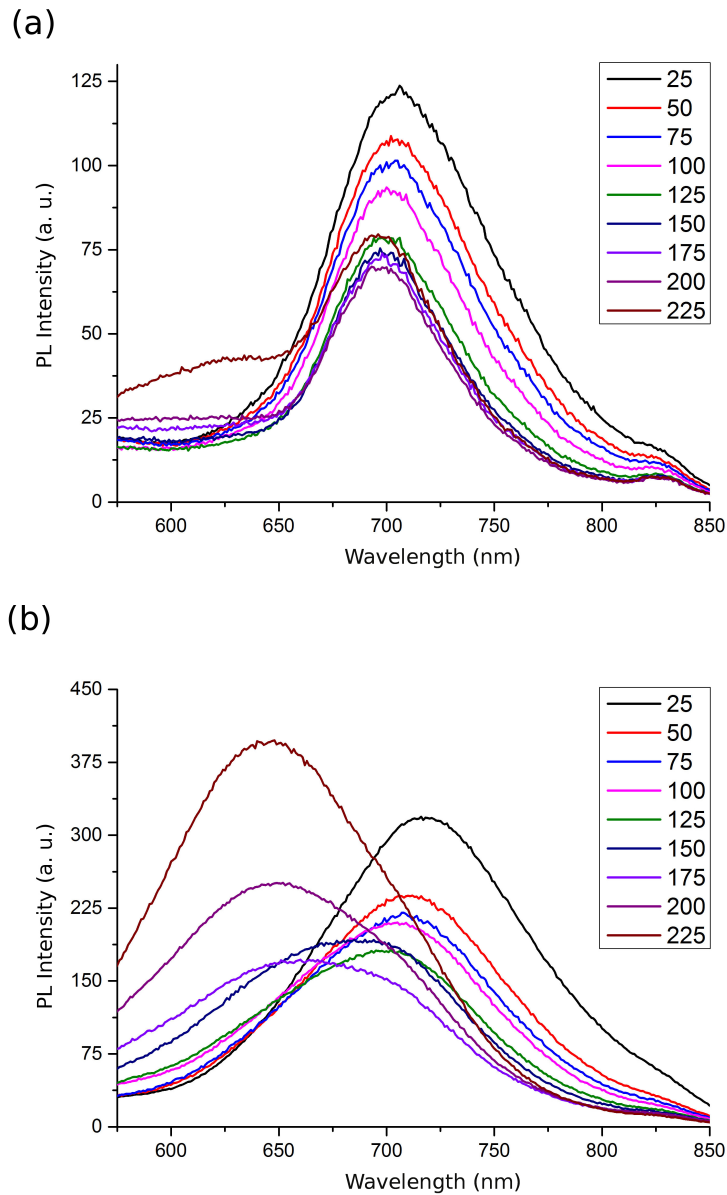


Figure 3.7: Measured PL intensities of free standing silicon nanocrystals on a quartz wafers with varying temperature from different samples. (Temperatures are in centigrade ($^{\circ}\text{C}$) degrees.) (a) The first sample prepared by dip-coating method. (b) The second sample prepared by same method and from same Si-Nc solution. Increasing temperature initially decreases the intensity then it shifts toward smaller wavelengths and increases, which is known as blue shift. The difference between two figures may be due to samples which they are dip-coated. The size distribution hence oxidation rate is not same for two samples. However, their tendency and behaviour are similar eventhough it is not exactly same.

hindering losses from total internal reflection from surrounding glass matrix interface. Since the glass also have refractive index around 1.5, the emission efficiency can be increased with a host which has even slightly larger refractive index, which is polycarbonate in our case. A second consideration was the low drawing temperature, due to the low glass transition temperature. Since the luminescence of the nanocrystal decreases with increasing temperature, the temperature exposure should be kept as minimum as possible. Hence, polymers which can be drawn at relatively low temperatures are the most suitable ones. Among these polymers, polycarbonate was one of the best choices due to its glass transition ($T_g = 147$ °C), and drawing temperature which is around 220 °C, for our design.

After this selection stage, a second decision about the starting point of the preform preparation were made. The original plan was to produce cylindrical shaped doped polymer rods with dissolving films, then mixing with silicon nanocrystal and finally pouring this mixture into a cylindrical glass mold. These trials were failed to give desired doped preform because the solvent (DCM) used to dissolve polymer films were highly volatile leading to form of a thin film layer between mixture surface and air. This thin layer prevented the formation of cylinder with removal of the solvent, whereas several thin layers took place instead of forming a cylindrical geometry. A second problem was the capillary effect of the glass mold that is the liquid mixture tends to stick to inner surface of the glass mold. This tendency leads to a non-planar, bell-shaped liquid surface-air interface which is problematic for well-shaped cylinder formation. It should be mentioned that there is a way to build such a cylinder with using PMMA pellets after mechanical and thermal treatments [51]. However, since we try to introduce a new method which will also work for other polymer sets, we didn't choose to repeat this method. As we will see, our design is superior to this method since with our method any type of polymer can be used for such a doping procedure.

A second choice for the work was the production of the silicon nanocrystal doped polymer thin films. After failing at the production of cylindrical doped preform with above mentioned method, we originally developed a new method to realize this. The starting point was the production of large area, thin, doped films which already constitutes important and popular research fields [11, 70, 71].

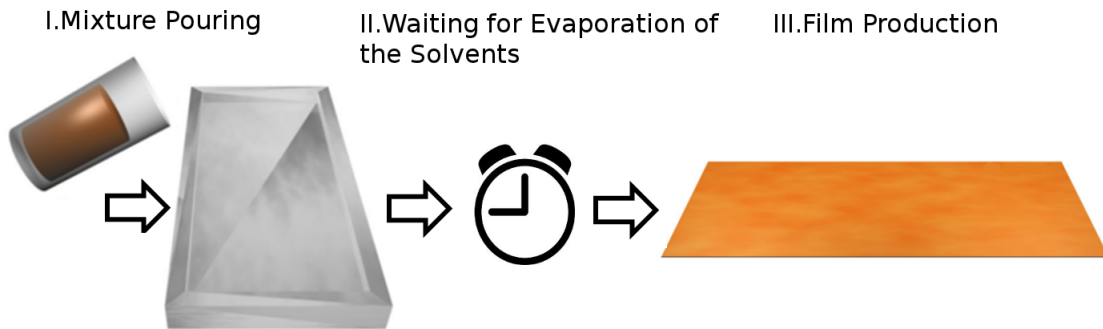


Figure 3.8: Schematic representation of the doped thin film production. Corresponding solution of the desired content is poured into the rectangular mold. Then, doped thin films are yielded after waiting for the evaporation of the solvents.

Here, our design includes a more general active material embedding procedure for producing large area loaded polymer films but since our main consideration was producing nanocrystal doped nanowires with using loaded films, we didn't focused on this. After several trials of film production, the procedure was optimized. Optimized doping procedure consists of several steps. First, as mentioned before, the choice of the polymer was an important part of the design since the polymer should not have absorption on corresponding wavelengths and have a refractive index similar to glass in order to extract more photons from glass matrix surrounding nanocrystals, which increases external quantum efficiency. Also, the polymer should have protective properties for some environmental effects such as oxidation and temperature. Hence, after trials with different polymers, polycarbonate films were chosen to be the most suitable one whose glass transition and drawing temperature are lesser than other available counterpart polymers. Consequently, doped (PC) films were prepared by dissolving a commercially available PC sheet with dichloromethane (DCM) and subsequently Si-Ncs with its host(pentane) were added to this solution. After mixing with magnetic stirrer for several hours, the mixture was poured to the rectangular stainless steel molds (with sides length 17 cm and 8.5 cm) and waiting for an overnight drying period, the solvents in the mixture (DCM and pentane) were removed by evaporation, yielding to a Si-NC doped PC film (Figure 3.8). The bright luminescence can be seen in the Figure 3.9, which proves that our procedure is nondestructive for

luminescence of silicon nanocrystals. The simplicity and success of this method make it a good alternative for the production of such doped films. The method can be the main topic of another work but here our main aim is to produce doped nanowires, we leave it at this stage, which can also be improved in future works.

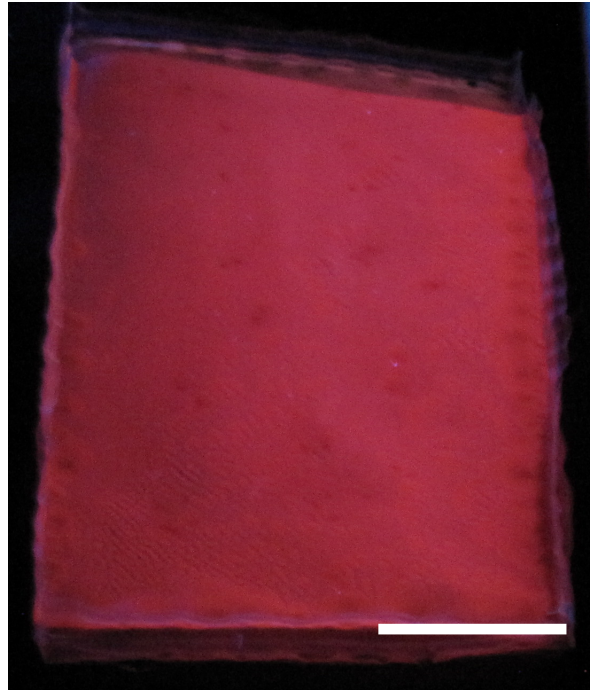


Figure 3.9: Image of silicon nanocrystal doped thin polycarbonate film under UV illumination. Red color of the film is due to dopant silicon nanocrystals where the excitation wavelength was 325 nm. The scale bar corresponds to 3 cm.

The temperature dependence of luminescence of the films were analyzed with heating different samples cut from the same film up to different final temperatures from room temperature to 225 °C by increment of 25 °C for the comparison with free standing Si-Nc and to see the effect of doping. We previously showed the effect of increasing temperature to free standing nanocrystals in Figure 3.7. The figure shows the gradual quenching of luminescence from free standing nanocrystals, with blue shift at high temperatures due to oxidation of nanocrystals. On the other hand, polymer embedding gives protection to oxidation with preventing the crystals to exposure of oxygen in air. Another mechanism, change of refractive index of polymer with increasing temperature [72], also plays an important role on external efficiency. Hence, the cumulative effect of thermal treatment was

intensity increment, due to efficiency enhancement, and PL shift, due to size reduction. Figure 3.10 shows this relationship, with curves showing PL intensities and with inset UV images, respectively. The maximum measured intensity of the luminescent films was at 150 °C since at this temperatures glass transition occurs resulting to refractive index change. This analysis also shows that at the consolidation (180 °C) and drawing temperatures (225 °C), the luminescence remains and gives chance to produce luminescent fibers with thermal drawing.

To sum up, with our new design we made a contribution to the field of large area film doping where there are already several approaches available in literature [11, 70, 71]. Yet, in our study we chose a totally new polymer for doping which is excellently suitable for repeated thermal drawing and which can be also drawn with a chemically inactive polymer (PVDF) which will be used as protective layer for doped core when chemical removal of cladding PC layer. As an alternative and simpler way of doping polymer films, our method consists of dissolving of the content with relevant solvents, mixing them and evaporation of these solvents. This method is considered as a new, simple, alternative method for producing polymer films doped with active materials.

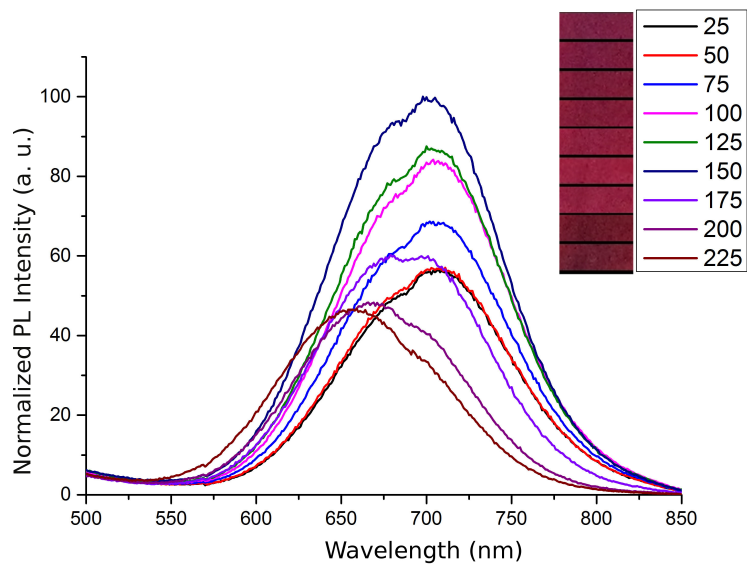


Figure 3.10: Measured PL intensities of the doped film with varying temperature and corresponding photographic images (inset). PL intensities increases up to 175 °C then reduces, with increasing temperature. The trend can be seen in photographic image. However, another phenomena known as blue shift takes place when the temperature reaches to 175 °C. Also, the maximum of the measured intensities occurs at 150 °C, which is thought to be due to refractive index change of the surrounding polymer which has glass transition around 150 °C.

Chapter 4

Silicon Nanocrystals Embedded Micro- and Nano-Structures

As a design under consideration, quantum dot decorated or doped nanowires have already been worked by many researchers for many different goals like increasing emission efficiencies, controlling emission directions or single photon extraction [5, 16, 46]. All these structures have their way to demonstrate the concept behind the works but they all have some drawbacks such as limited production length, experimental complexities, positioning and alignment difficulties. Within these structures fiber geometry is the common crucial point, yet, wafer based or chemical based fabrication techniques have some drawbacks for large area applications and applications which requires high control on the geometry [52]. Besides, thermal drawing is versatile technique by which multi-functional nano-fibers can be produced, shaped and patterned with macro scale control tools. Hence, structured, decorated, doped or active material filled luminescent nano-fibers or nanowires can be produced for their high promising potential applications such as elastic displays, fiber lasers and single photon emitters [73, 74, 75] with thermal drawing since among the nanowire production processes, repetitive thermal drawing method has some advantages over other nanowire production methods like functionality, alignment ability, production simplicity and high throughput rate [8]. Also, since the technique should be suitable for such a functionalization

process, it is worth to mention that the procedure and the fabrication steps are very suitable for production of such an active material doped nanowires.

In this chapter, we state the method of producing Si-Nc doped luminescent polymer nano-fibers which are more functional due to its handiness, alignment ability and luminescent stability, by iterative thermal drawing method, with doped preform preparation, where silicon quantum dot synthesis and film doping were given in previous chapters.

4.1 Preparation of Macroscopic Preform

With iterative thermal drawing technique, it is possible to overcome some of above mentioned difficulties and get a chance of producing new geometries which have not been realized yet. Also, with this mechanism not only Si-QDs but also other dopants such as magnetic nanoparticles, dyes, other types of QDs can be easily embedded into the nanowires for both applications and research purposes. In order to perform this doping procedure, we started with the macroscopic preform design. The macroscopic preform consists of two main components and three layers. It is basically a rod having a nanocrystal doped core and undoped cladding in its geometry axis. Also, a thin layer of PVDF between core and cladding is added to prevent the doped core from chemical etchants which will be used for removal of the cladding. A schematic picture of the cross sections of the macroscopic preform is given in Figure 4.1. In order to realize this design, we firstly tried to prepare the doped core.

In the preparation of the doped core preform we did several trials in order to produce it directly with dissolving host polymer with a relevant solvent, mixing with dopant solution and evaporating the solvents in a cylindrical glass mold. However, these trials were failed due to high volatility of the solvents and capillary effects occurring between the mixture and surface of the glass mold. The high volatility of the solvents caused to formation of thin layer between surface of the mixture and air. Then, it continued the behavior in the same manner and the

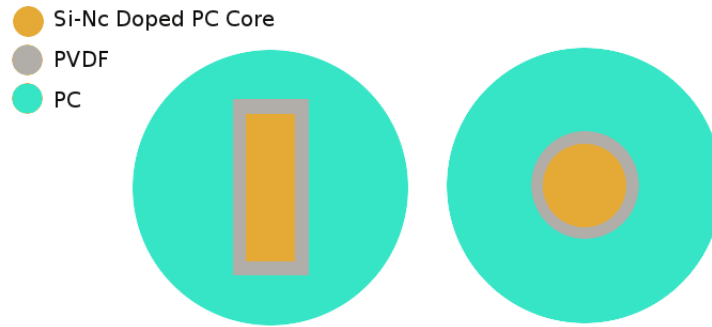


Figure 4.1: Schematic illustrations of cross sections of the designed fibers. The geometries consist of core/cladding structure and a thin PVDF layer for protection of the core during chemical etching of the cladding

result was several layers of thin films with some non uniform distance between them. Also, capillary forces give rise to a bell shaped interface between surface of the mixture and air and the resultant preform has empty regions and holes in its geometry. We tried several chemical and physical methods in order to minimize these effects. Firstly, we tried to make evaporation more slower by using filters in open ends of the mold. Yet, this did not work. It only extended the solidification time and made films thicker.

After these failures, we changed our route. Since we have had previous experience with producing preforms from polymer films, we tried to produce doped films then doped preforms. A detailed explanation of the preparation of the doped polymer film was given in chapter 3.3. Here, we will explain the doped preform preparation. After production of the doped films, firstly we produced a rectangular rod with rolling the doped films around themselves and shaping it with sandpapering after consolidation. Figure 4.2.a shows the resultant doped preform. Its bright luminescence (Figure 4.2.b) shows that even after consolidation, high temperature solidification of the preform, the luminescence still be kept. After this successful results we passed to next step.

The next step was the preparation of the final preform which will be drawn with thermal drawing. We started this with rolling several layers of PVDF films around doped core which is followed by putting this into another preform which is prepared with tightly rolling undoped PC films around a cylindrical glass rod

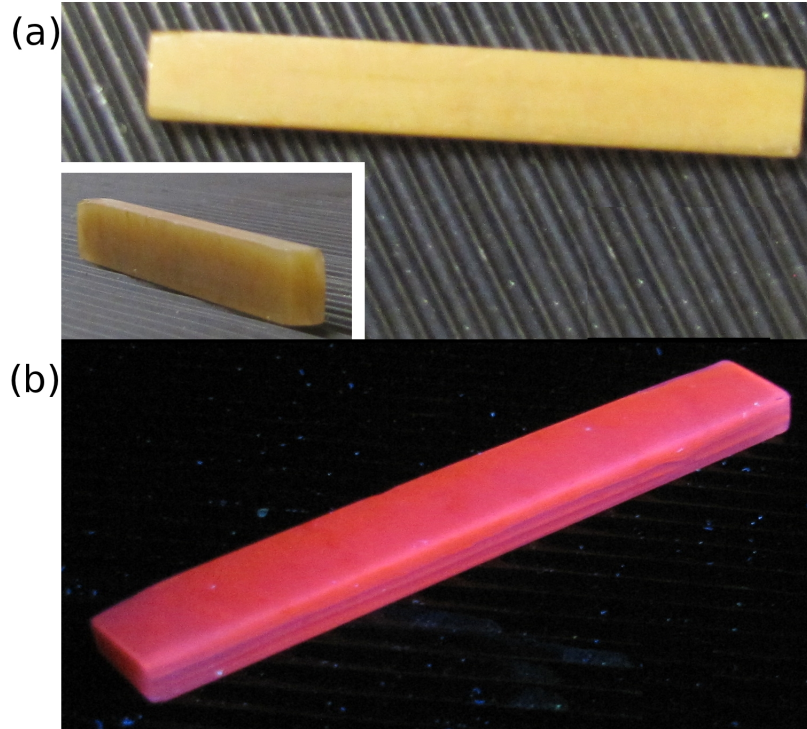


Figure 4.2: Rectangular doped core preform. (a) Bright field image of the core and (b) UV image of the same. Red luminescence can be seen in latter image which shows consolidation process does not harm luminescence of the silicon nanocrystals

until the desired size was reached. After this rolling, the preform was consolidated at 180 °C for 2 hours. Then, the cladding preform was divided into two parts and a rectangular hole was carved on these two parts (Figure 4.3). The dimensions of the carved regions were adjusted to the dimensions of the doped core with surrounding PVDF layer, just fit into the hole. Then, the whole structure which consists of two sides of cladding preform and core preform with surrounding PVDF was capped and consolidated at 180 °C. After this treatment, we finally get the desired doped core macroscopic preform. Also, eventhough the core was rectangular, the final preform was cylindrical which is also more desired for uniform distribution of heat during thermal drawing. Figure 4.4 shows the final shape of the preform.

Another type of preform which has cylindrical doped core, was prepared with a slightly different methods as illustrated in Figure 4.5. Firstly, doped films were

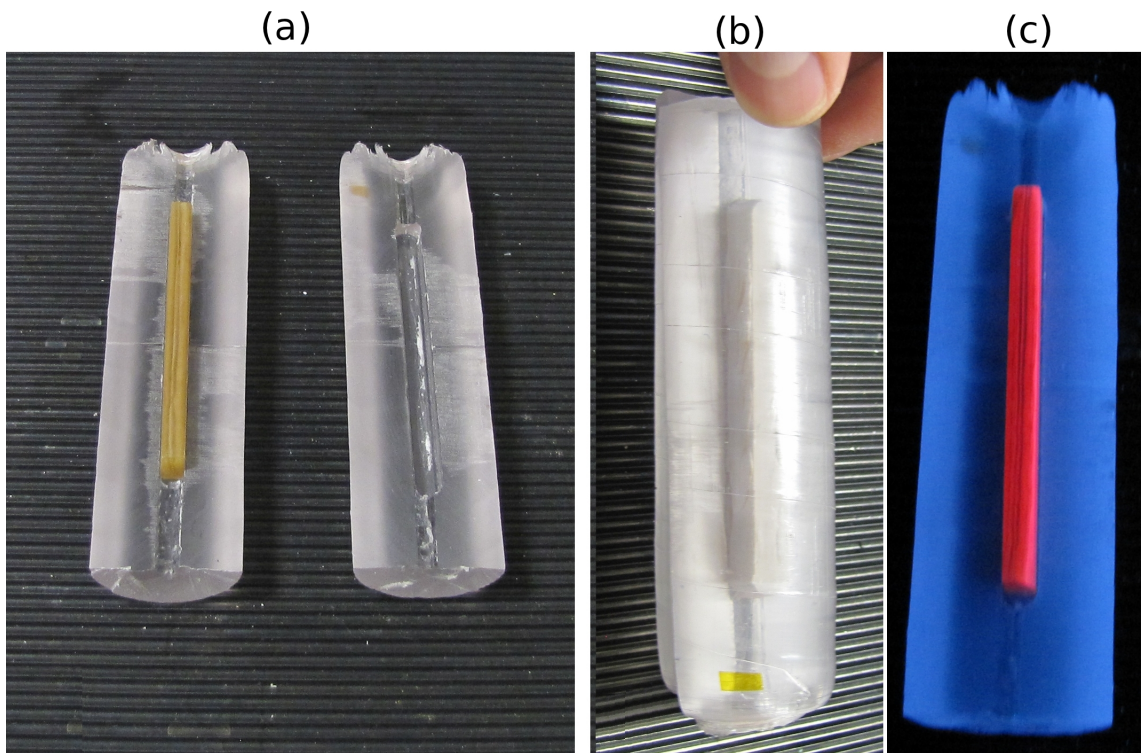


Figure 4.3: Subdivided and carved PC preform. Rectangular carved regions are adjusted to just fit to doped core. (a) Image of the preform with doped core placed in the hole. (b) Capped of the same. (c) UV image of the same.

prepared as explained in Chapter 3.3. Then these films were cut circularly and filled in a cylindrical glass mold. This structure was consolidated at $180\text{ }^{\circ}\text{C}$ in vacuum during applying mechanical pressures from both ends. Finally, doped core preform was held after removing of the glass mold (Figure 4.6.a). Figure 4.5 summarizes the procedure. Also, we can see the bright luminescence of the doped core in Figure 4.6.b. Subsequently, several layers of PVDF followed by undoped PC layers were tightly rolled around doped core up to a final predetermined diameter size and as a whole this structure were consolidated again (Figure 4.7). The final preform is shown in Figure 4.8.a. The dimensions is also shown in Figure 4.8.b.

The method used for the production of the doped, cylindrical core is a simple but a new method which was very successful since the final shape was quite good. With this method, the production of such a doped preform with a convex



Figure 4.4: Consolidated rectangular doped core preform and final form of it which is stuck to adapter preform before drawing.

shape can be made with some modifications and with a relevant mold. For a research, it is important to introduce new alternative production techniques for the development of the corresponding field. Here, with this design we present totally a new solution for the production of such a doped preforms.

In this work, we only synthesized red silicon nanocrystals and films doped only with these nanocrystals. However, we got other colors with chemical etching of the doped cores and fibers. We noticed this by accident. In most cases, the glass mold used for the production of the doped core can be removed mechanically after consolidation. However, in some cases, some amount of glass pieces can stick on the polymer used for doped preform. In these cases, we use chemical agents in order to remove these pieces. During the chemical removal of the glass mold used for doped core by HF etching, we accidentally noticed that the solvent (HF) penetrates to the doped core. Hence, the dopant nanocrystal size were reduced and subsequently the color shifted to the smaller wavelengths. Figure 4.6.c shows the result of this treatment. The doped preform were illuminating red before the treatment, but after the treatment it turned out to yellow. However, we also noticed that the color got with this method was not stable and it quenched after some time. The reason behind could be that the solvent may not be completely

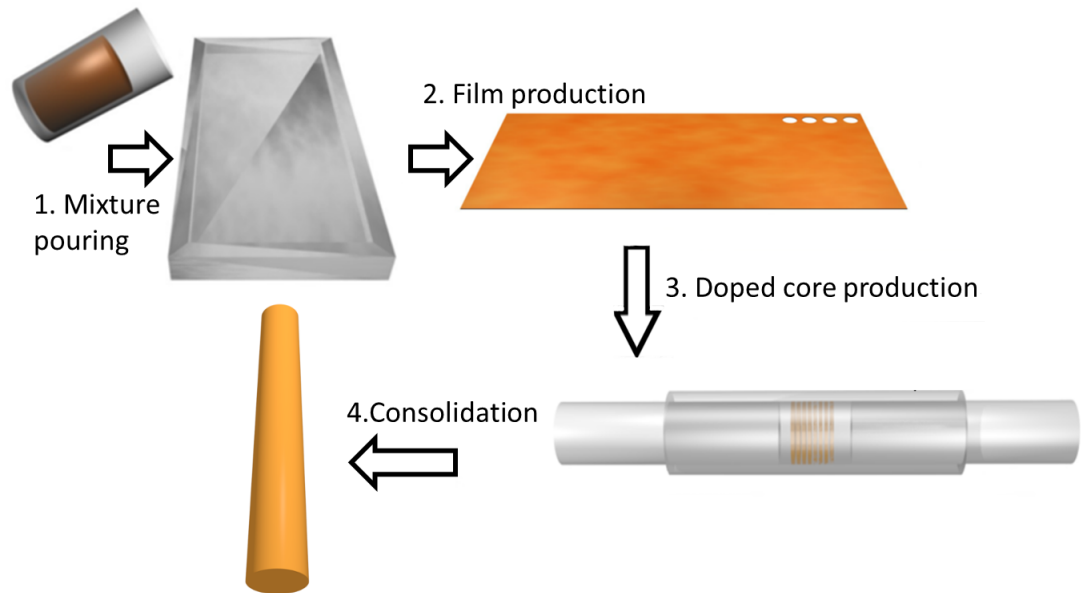


Figure 4.5: Schematic representation of cylindrical doped core preparation. The first three steps are doped film preparation as explained before. Doped preform preparation steps are cutting doped films into circular pieces, filling them into a cylindrical glass mold, consolidation and removing the mold.

removed from the doped core after the treatment and residual solvents inside the preform etches the nanocrystals more with time. Eventhough, this treatment has some drawbacks, it is a new method which can be developed further, for the production of colored preforms and fibers.

4.2 Production of Core-Shell Nanowires by Iterative Size Reduction Technique

Throughout this work, the fibers are fabricated by thermal drawing of a fiber preform [8]. The drawing was performed by a fiber tower (Figure 4.9) by which the drawing parameters (temperature, drawing and feed speed) can be simultaneously controlled, during drawing. Since each material set have different time and temperature requirements to flow and to be drawn, the drawing parameters

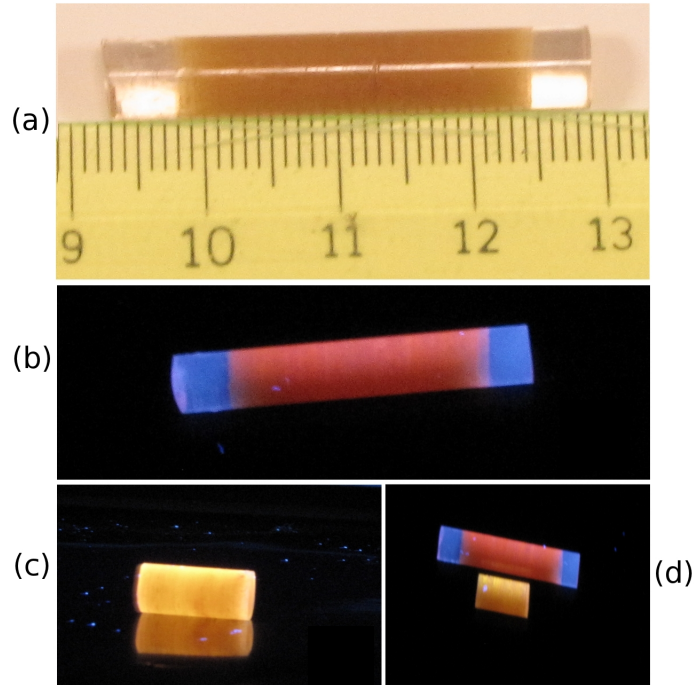


Figure 4.6: Images of the silicon nanocrystal doped PC core preform. (a) Bright field image of the core. (b) UV image of the same. (c) Another doped core preform obtained from the post-etching method which causes red color to turn into yellow. (d) Another UV image of the core preforms

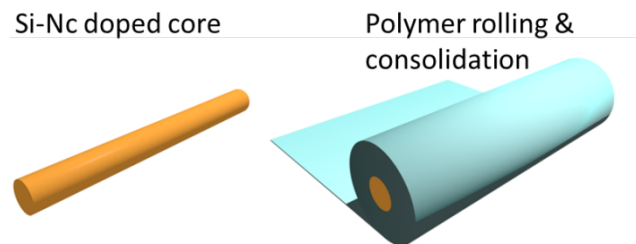


Figure 4.7: Preparation of a preform. Several layers of thin polymer films are tightly rolled around the doped core until the desired dimensions are held. Then, with thermally treating this structure, it is consolidated and becomes the final form before drawing.

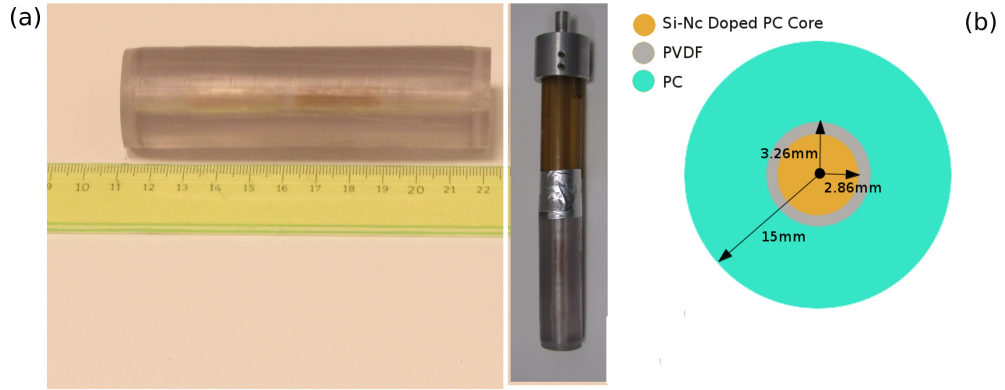


Figure 4.8: Final form of the cylindrical doped core structure and corresponding sizes. (a) Consolidated preform. (b) Corresponding core/cladding dimensions.

should be precisely adjusted. Also, the preform geometry affects temperature distribution and drawing forces, thus both the material and the geometry should be considered carefully for adjusting drawing parameters. For this work, the heating regime was between 220 °C and 240 °C depending on the tensional forces on the fibers during drawing. These temperature regime is determined by the material properties of PC and the core/shell geometry of the fibers (Figure 4.1).

Thermal Drawing

The actual mechanism of the thermal drawing is quite complicated. However, for a deeper understanding, an accurate physical explanation can be made with several simplifications like reducing the explanation to conservation of mass problem. Also, with making further assumption of constant material density during drawing, the problem turns into conservation of volume. Hence, a relation for fiber drawing speed (v) can be given as,

$$v = \frac{R_{\text{out}} - R_{\text{in}}}{r_{\text{out}} - r_{\text{in}}} V$$

where, V is the feed speed, R_{out} and R_{in} are outer and inner diameters of the preform, respectively and r_{out} and r_{in} are outer and inner diameters of the fiber, respectively. However, in case of great difference in density of materials between core and cladding, we should amend the formula. Hence, with defining two parameters collapse and rescale factors as,



Figure 4.9: Computer controlled fiber tower facility and its schematic diagram

$$R = \frac{r_{\text{out}}}{R_{\text{out}}}$$

$$C = \frac{r_{\text{in}}}{R_{\text{in}}R}$$

then the speed expression can be redefined as,

$$v = V\lambda$$

$$\lambda = \frac{1 - \alpha}{R^2(1 - C^2\alpha)}$$

where,

$$\alpha = \left(\frac{R_{\text{in}}}{R_{\text{out}}}\right)^2$$

Then the total length of the fiber (l) will be,

$$l = L/\lambda$$

where L is the preform length. This simplified explanation works quite good for materials that their density does not change much with changing temperature. Also, eventhough it is not exact, the mechanism can be understood better within this perspective. Hence, During drawing, the drawing parameters (temperature, feed speed, drawing speed) can be adjusted with using above equations in order to get desired fiber sizes.

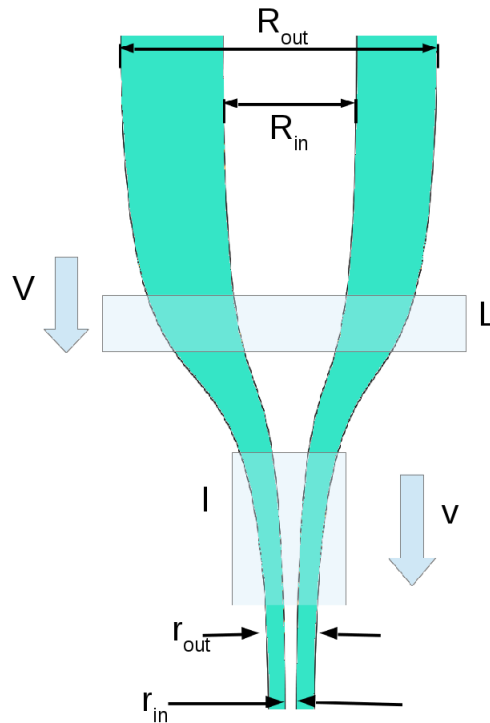


Figure 4.10: Illustrative drawing explaining the parameters of thermal drawing. The parameters are defined as in the text.

Iterative Thermal Drawing

Our iterative thermal size reduction method (Figure 4.11) consists of several repeated drawing of polymer preforms filled with fibers from previous steps [8]. Final structure is always determined by design and geometry of the first step preform. The shape of this preform is preserved while drawing, whereas the

dimensions will be smaller and smaller in each step. Depending on the size reduction ratio any fiber with any size from a few millimeters to a few nanometers can be produced with this method. For the first step fibers, a fiber preform having dimensions of a few centimeters is drawn thermally. During this drawing with changing temperature, feed and drawing speed, fibers having several different dimensions can be achieved from the same initial preform. Depending on the polymer type and preform geometry, the size reduction ratio, can be as little about 10 and as much about 250. Hence, any desired dimension can be fabricated by proper adjustments of the drawing parameters. Also, since the drawing reduces the perpendicular dimensions, it increases parallel dimensions with drawing forces. Hence, from only a few centimeters long preform, one can get hundreds of meters fibers.

For this work, the first step fibers were drawn from the preform which has a structure that is explained in the previous section. The drawing was conducted with following standard procedure which is explained above. The drawing temperature was 220 °C. Also, feed speed and drawing speed were adjusted to get desired diameter size for the first step fibers. We started with producing a few millimeter fibers and subsequently reduced the size gradually to several hundreds microns. Hence, even in one step, we got fibers having different dimensions from the same preform. In addition, depending on the size reduction ratio, the doped core size was also reduced. Hence, with only one step, we reduced the dimensions of the doped core to tens of microns. In Figure 4.12.a, the first step fibers from a rectangular preform are shown. They were not good enough to be used in next steps since the geometry of the preform were distorted during drawing because of the defects on the preform. On the other hand, cylindrical fibers (Figure 4.12.b) drawn from cylindrical preform preserved its geometry and they can be used in next steps.

As we stated above, with thermally drawing cylindrical preform we got our first step fibers which were hundreds of micron sized, actually around 350 μm . The drawing process repeated with filling a prepared PC hollow core preform with several hundreds (around 250) of first step fibers which results to reducing of doped core size to nano dimensions (Figure 4.13). Hence, after two step drawing

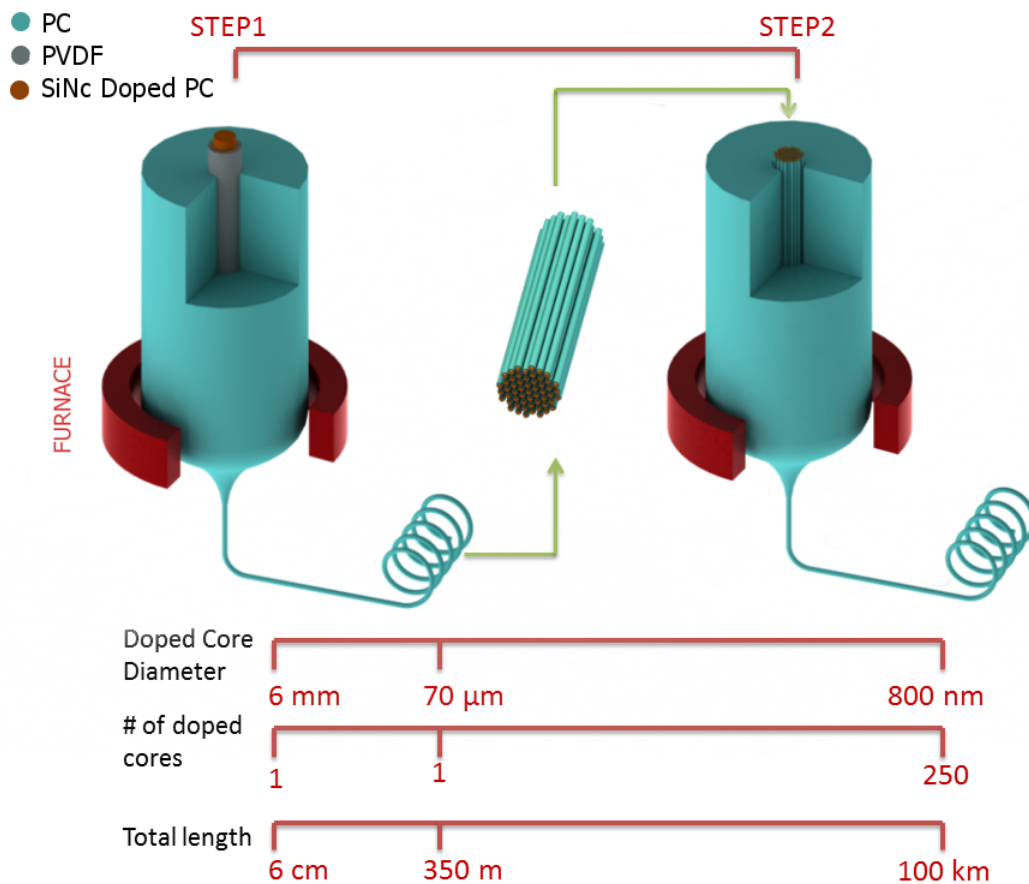


Figure 4.11: Schematic illustration of iterative thermal drawing technique. With repeated procedure it is possible to get kilometers long, nanofibers. Here another crucial property is the array structure. The array can consist of hundreds of antecedent fibers.

we got desired dimensions and we did not go further for third step. However, if desired, it is straight-forward to draw third step fibers from second step fibers with filling and drawing another hollow core preform. Yet, since we try the proof the concept we did not do further drawing for this work. At this step, they also preserved their cylindrical geometry and the length elongated from an initial a few centimeter preform to total length of kilometers of nanofibers. Also, the array of first step fibers in the second step fibers formed a hexagonal structure like honeycomb lattice due to tendency of maximum filling of the empty volume. Hence, with only two step drawing we got kilometer length, array of silicon nanocrystal doped nanowires which is shown in Figure 4.13.

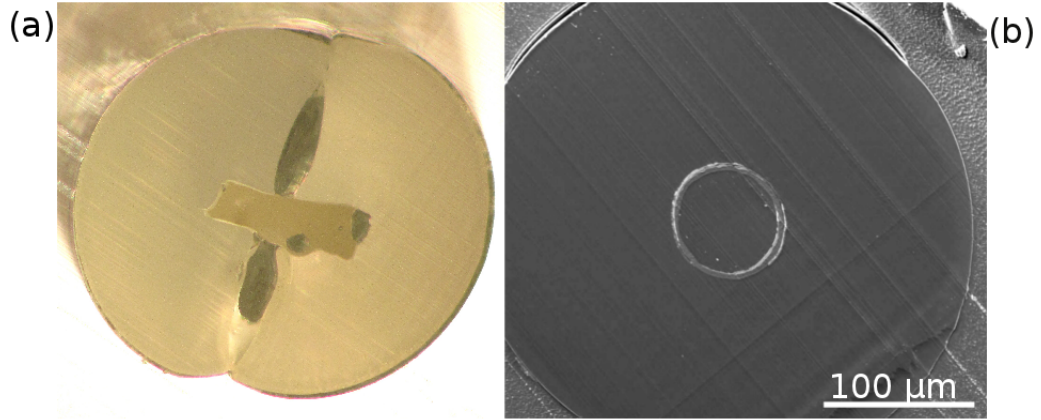


Figure 4.12: The first step fibers. (a) Bright field microscope image of rectangular doped core fiber and (b) SEM image of cylindrical fiber.

With this work, we originally proposed and realized nanostructured fibers with iterative size reduction technique. This approach differs from similar previous works which uses thermal drawing method [47, 51], mainly at three points. First difference is the choice of the active material and enclosing polymer. We selected the Si-Ncs due to the reasons mentioned above rather than heavy metal (CdSe/ZnS core/shell) QDs. Our choice for enclosing polymer was PC rather than polymethylmethacrylate (PMMA) and our procedure permits the use of other types of polymers (Polysulfone (PSU), Polyethersulfone (PES) *etc.*) as well. Second difference is regarding the procedure that, our starting point was producing large area nanocrystal doped luminescent films which were used to produce doped cores by stacking in a mold, whereas previous works directly produces doped cores and surrounding preforms by mixing QDs with PMMA chemically, and then, after removing the solvent, the preform is fabricated by mechanical powdering and thermal molding. Third, the final fibers in this work are two orders of magnitude thinner than that of previous works [47, 51]. Also, comparing to electrospun doped nanowires; our design has superiority at alignment, controlled and non-complex resulting geometries. A more complete comparison of the nanowire production techniques is given in Table 4.1. All the mentioned methods in the table have some advantages and disadvantages from several aspects. The choice of the production method is very dependent on the requirements of corresponding design. Yet, with this work, we introduce a new approach which combines highly

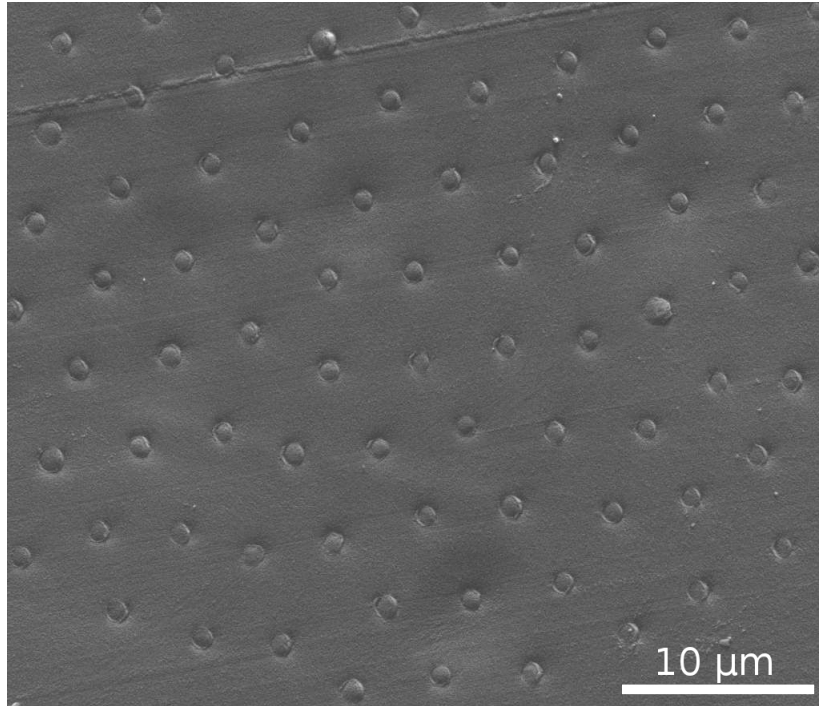


Figure 4.13: SEM image of cross-section of second step doped fiber. In the second step, doped core diameters were reduced to nanodimensions.

demanded features of production steps and of resulting nano-geometries.

4.3 Characterization of Nanostructures

A deeper understanding of the success of the proposed design can be understood better with relevant measurements and corresponding analysis. Hence, for this reason, we did several measurements on the fibers in each step. In order to see, final geometry of the fibers we took SEM images of both cross-sections and side views. Also, with measuring photoluminescence we can compare and evaluate the success of the method for producing luminescent nanowires. In addition, images taken under UV illumination shows the success rate in a more direct manner since one can observe the results with bare eye. Hence, the fibers produced with iterative size reduction were characterized with several measurements and observations, and the results were carefully analyzed. For this work, we have two

Table 4.1: Comparison of doped nanowire production methods from several aspects

Properties\Methods	ISR	Electrospinning	Clean Methods	Probe Drawing
Size(diameter)	micro to nano	micro to nano	nano	nano
Handling\geometry	simple handling,non-complex geometry	simple handling,complex geometry	hard handling,non-complex geometry	simple handling,non-complex geometry
Maximum length	km	km	μm	m
Concentration	high	high	low	high
Production simplicity	simple	simple	hard	simple
Uniformity of the nanowires	high	moderate	high	moderate

type of fibers, one with rectangular core and one with cylindrical core. Also, for cylindrical fibers we have two step products.

For the fibers with rectangular core, we took UV images and cross-section images. In Figure 4.15.b, the luminescent cross-section under UV illumination can be seen and in Figure 4.12.a the cross-section microscope image is shown. In these images, eventhough doped core gives bright luminescence, it can be seen that the geometry of the fiber is distorted. At the intersection surfaces, empty regions can be seen, which is due to defects on the first step preform. The rectangular geometry of the core were not preserved. However, they prove that even in such high temperature drawing photoluminescence from dopant nanocrystals remains. The defects in the first step preform were thought to be caused from microscopic mismatches at the interfaces. Also, the rectangular doped core and the carved regions in the host preform were not perfect rectangles. Thus, these imperfections may cause to resulting fibers shown in Figure 4.12.a. At this work, only red colored rectangular fibers were produced but as mentioned before the procedure holds for other colors, as well.

Highly ordered first step fibers are shown in Figure 4.14. Also, the luminescence from first step doped cylindrical fibers produced with iterative size reduction can be seen in same figure. Furthermore, luminescent cross section is given in Figure 4.15.a with PL measurement given in Figure 4.16. These results shows

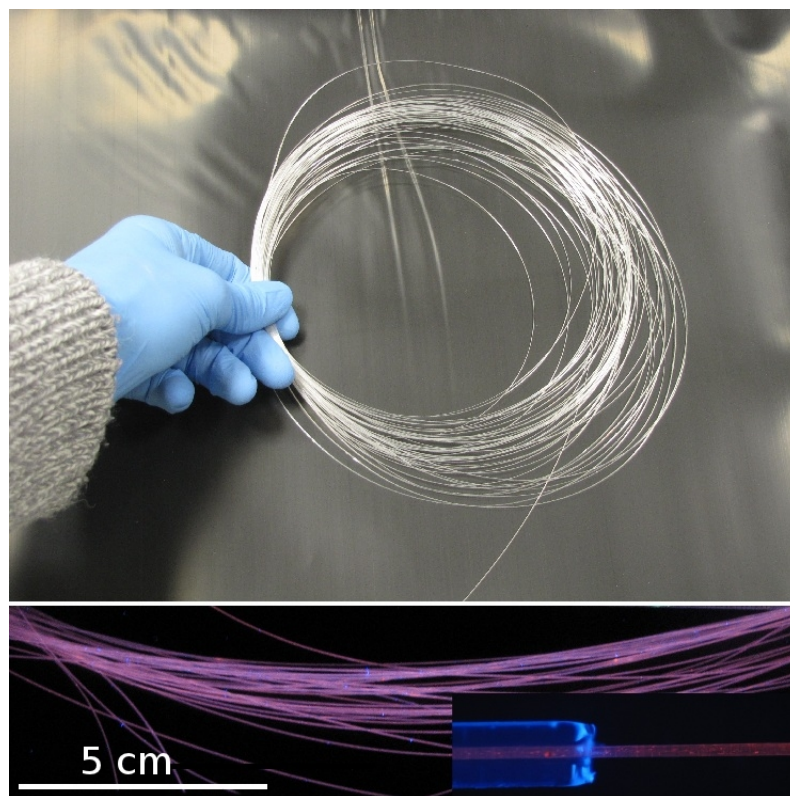


Figure 4.14: Highly ordered first step fibers that are thermally drawn and their red luminescent UV image. In the inset the luminescent core can be seen. This non-complex geometry is important for applications which needs precise and simple control.

that for the cylindrical geometry, the procedure also works. Contrary to previous rectangular fibers, the cylindrical fibers has nearly perfect geometry which shows that in this design the preform geometry is conserved (Figure 4.12.b). Also, the bright luminescence both from side view and cross-section shows during the drawing photoluminescence is not affected much from temperature. Also, a smaller blue shift seems to have occurred. However, the fibers protects the dopants from total oxidation and prevents photoquenching. Also, in order to demonstrate the usability of the fibers, we wrote the name of our institute with our luminescent fibers (Figure 4.17.a), which was taken by optical microscope camera with UV florescent lamp illumination. The figure clearly shows the alignment ability and usability of our fibers. Also, other colors rather than red were achieved with totally different manner. As mentioned before, the HF can penetrate into the fiber and depending on the reaction time any color can be got from red fibers. The

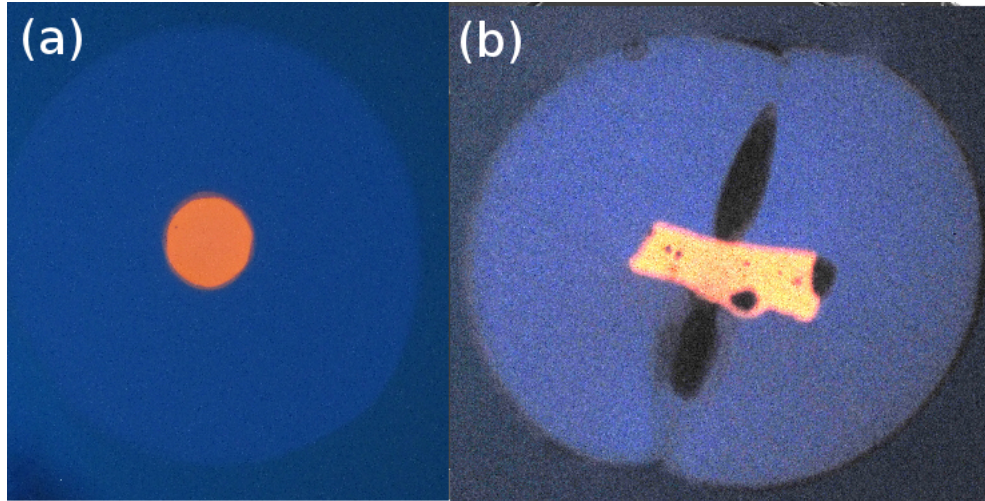


Figure 4.15: Cross sections of first step fibers. (a) UV image of cylindrical core fiber. (b) UV image of rectangular core. Bright red colors can be seen at the core regions.

results can be seen in Figure 4.17.b and c. The yellow and green colored fibers were produced with this method. However, since the removal of the residual HF is problematic, the colors were not stable for long time. Yet, although the colors are not stable, it can be stabilized with finding a technique for removing the residual HF. This result is the second important result of this work since with such a simple treatment we can get different or multi colored fibers from only one type of colored fibers.

The luminescence from second step fibers was shown in Figure 4.18.a. Also intensity measurement was given in Figure 4.18.b which proves the clear luminescence from array of indefinitely long nanowires. There is a difference between peak positions of the first step and the second step PL intensities. This difference could be due to difference in sample preparation stages. The first step fibers inside the second step fibers might be took from different sections of the first step fibers which have luminescence at different wavelengths. The big, brighter points in the UV image are consequences of non-uniform size distribution of silicon nanocrystals but the fibers still keeps their geometry. It should also be noted that the second step can be drawn with including only one first step fiber inside instead of array of hundreds of first step fibers which may be tried for future designs. The

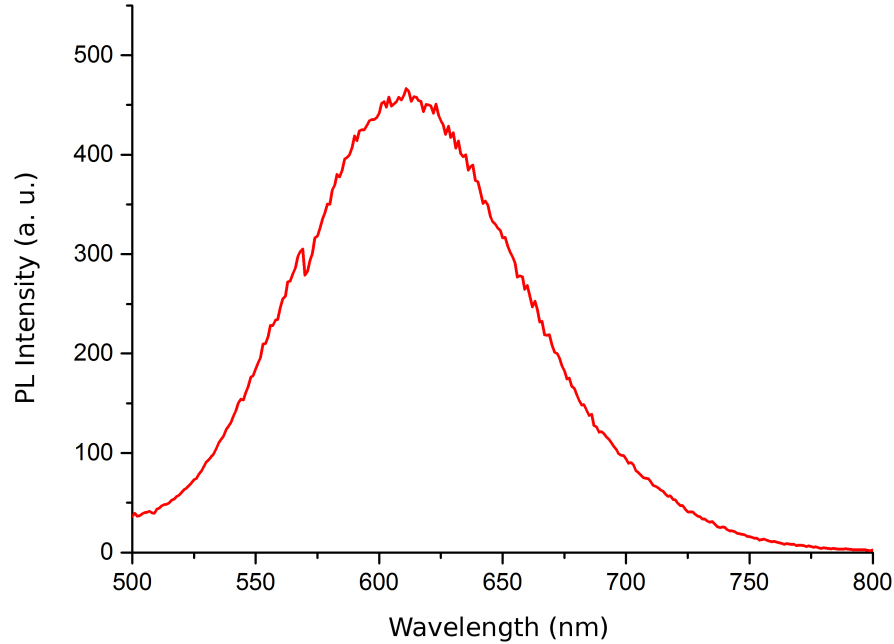


Figure 4.16: Measured PL intensity of the cylindrical core fiber. The peak positioned at 610nm and it proofs orange-like color of the first step fibers.

SEM images of both bundled nanowires and cross section are shown in Figure 4.19.a and 4.19.b, respectively. For the side view images, a bundle of the second step fibers were laid on wafer. Then, the undoped PC cladding was removed by etching with DCM solution. After the removal of the cladding, a bundle of silicon nanocrystal doped cores with surrounding PVDF layer was obtained. The cross-section shows the well-oriented array structure which includes hundreds of nanowires. Also, the side view image shows uniformity of nanowires along its elongation axis even though there are some sudden jumps where crystal matrix size is larger than the fiber diameter.

The above results illustrate the applicability of our method for producing luminescent nanowires. This method can be easily extended to produce other dopants embedded nanowires such as magnetic nanoparticles, dyes or other type of quantum dots. The resulted micro- and nano-wires shows luminescent properties which can be enhanced with optimized design. The results of this work shows

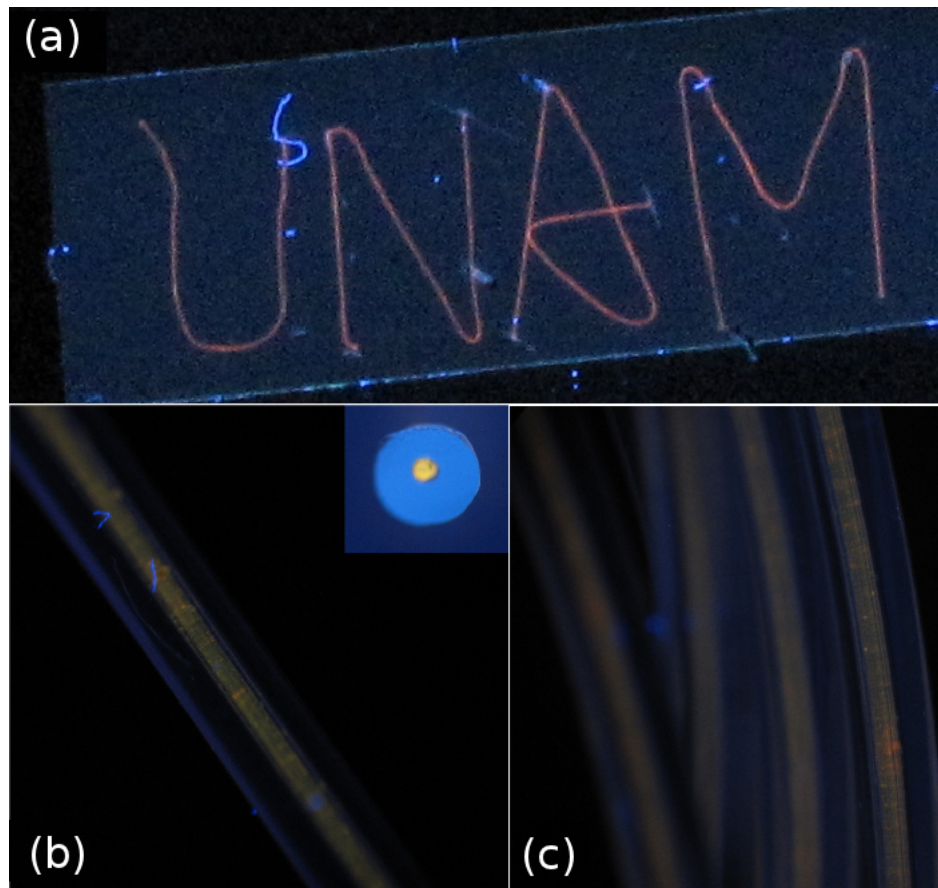


Figure 4.17: Images of aligned and colored Si-Nc doped polymer fibers. (a) The institute's name is written with luminescent cores. The image shows alignment ability of the fibers. (b) Green colored fibers which resulted from red luminescent fibers by HF etching treatment. (c) Yellow colored fibers which are also fabricated by a similar treatment but for a lesser treatment time.

that our method which is the production of nanostructured fibers with iterative size reduction technique can be used for any suitable nanowire/nanofiber doping, decorating and structuring processes. For the silicon nanocrystal dopants, it gave very successful end products. The success rate can be increased further with more careful production in each step. Yet, in this work we consider only critical points and applicability of the method so we leave further developments for future works.

For the applications side, we can count several technologies which already uses similar designs [22, 73, 76]. The doped nanowires produced in this work can

be used for fiber lasers, directional emitters, sensors, elastic displays, texturing and money security. Also, with optimizing the array structure it is possible to produce a 2D photonic crystal with embedded source which can be utilized for increasing luminescence or for guiding properties. With further size reduction and using more uniform and smaller sized crystals, it is possible to extract or to couple single photons from/to nanowires. However, the scope of this work was to show that iterative thermal size reduction method can be used in producing such doped nanowires; hence these above-mentioned improved designs are concerns of future studies.

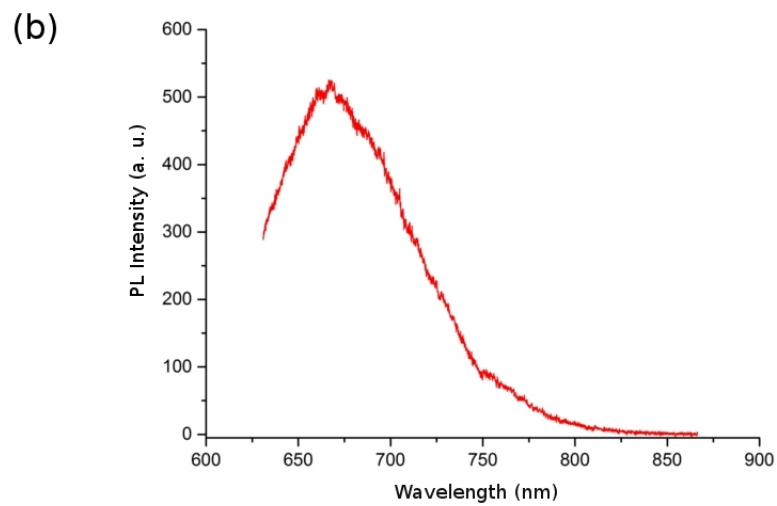
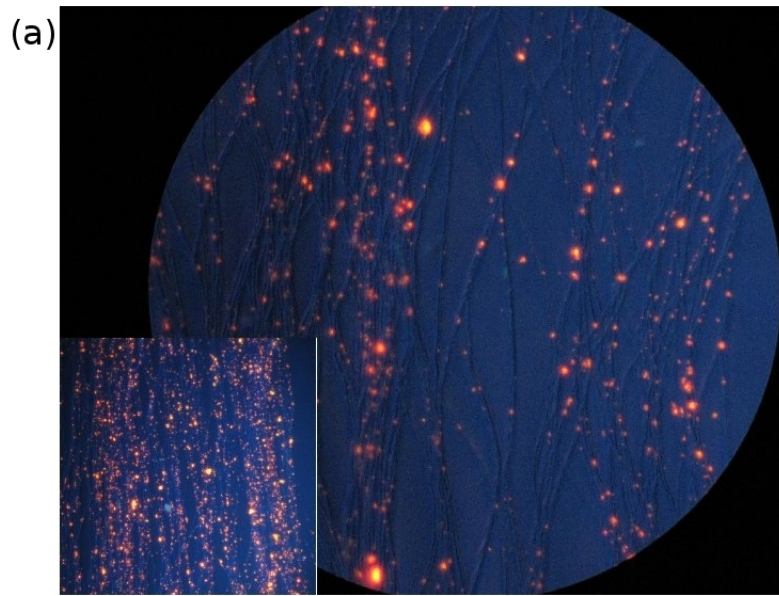


Figure 4.18: Luminescent microscope images and measured PL intensity of second step fibers. (a) UV image of second step fibers. Discrete luminescent points are the nanocrystal sites. (b) Corresponding luminescence measurement of second step fibers. There is difference in peak positions of the first and the second step fibers, which is probably due to samples gotten from different sections of the first step fibers.

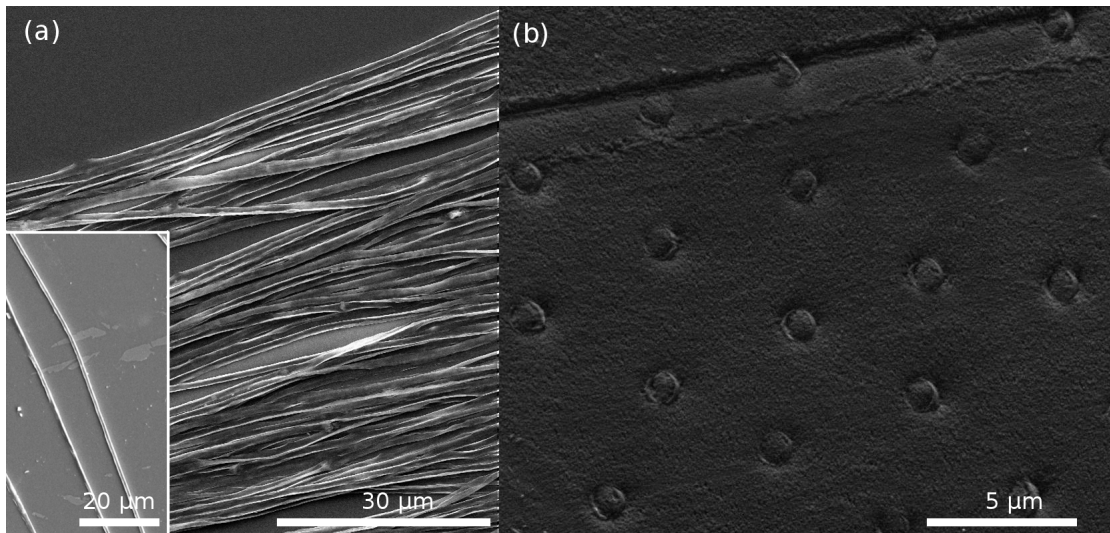


Figure 4.19: SEM images of second step fibers. (a) Side view. At some points, fiber geometries are distorted due to crystal size larger than fiber diameter. However, it still shows the applicability of the technique. (b) Cross-section of a second step fiber showing hexagonal packed array of antecedent step fibers.

Chapter 5

Summary and Outlook

Silicon nanocrystal doped nano-fibers have been produced by iterative thermal size reduction method (ISR), which gives the advantages of production ability of highly aligned, uniform; indefinitely long nano sized structured fibers illuminating at visible spectrum. Resulting fibers both as a proof of principle and as a route to new technologies pave a way to new research and applications.

Despite its advantages, the design and the principle have some challenges at this stage. The radial positioning of the dots inside fibers, non-uniform size distribution of crystals and the current intensity levels are three of them. However, as a proof of principle work, our design has a potential to be improved with future designs. For the future prospect, the design can be tuned and improved for the corresponding application such as 3D flexible displays, fiber lasers and optic sensors etc. Hence, this method addresses wide varieties of fields of research and can contribute to current state of the art technological design steps.

With this proof of principle work we showed that silicon nanocrystal doped luminescent nanowires can be easily produced and they have superior properties to other nanowires that are produced with other techniques. The choice of the dopant was the starting point of this work. One of the prerequisites for the dopant was that the dopant should have durable photoluminescence at high temperatures. Second property is that the luminescence should be protected during

doping procedure because the atmospheric oxygen threatens most of active luminescent materials resulting to luminescence quenching. Some trials have been made with commercially available CdSe/ZnS core/shell quantum dots but these trials failed to meet the above mentioned requisites. However, the experiment was done without any extra consideration and any development of the conditions in which the experiment was conducted.

At this point, we may use protective ligand capping for quantum dots. It is reported that these types of capping increases durability of the quantum dots to oxygen and high temperature exposure [77, 78]. However, the level of protection is not sufficient for our procedure and considering a replacement for the dopant was more appropriate choice. In addition, since one of the most important aspects of our design is the non-complexity of the procedure and keeping the experimental simplicity, for this work we did not insist on these type dopant and searched for the most suitable substitution. One of the most suitable candidates was silicon nanocrystals, since they had been produced several times in our research group before our current design. However, there were still problems with these type of nanocrystals. The non-uniform size distribution and agglomeration were two problem that should be solved before doping. For the first problem, shaking mixture of the silicon nanocrystal powder and glass beads made size distribution more uniform and reduced the average size. This treatment was sufficient for the current design and it has potential for future improvement but with paying a experimental complexity bill. For the agglomeration problem, the time between synthesis of the nanocrystal and doping step was kept as minimum as possible. Silicon nanocrystals were synthesized with these above considerations. The detailed information about the synthesis is given in Chapter 3.2.

After the choice and the synthesis, the next step was the film doping. We successfully doped and produced large area luminescent polymer films with our production method. The results of this step are as important as that they can be a topic of a paper or a thesis in itself but we gave it as intermediary result of our work since our aim was to produce luminescent nanowires. The main consideration about this step was the choice of the host polymer. The host polymer should provide protection to oxygen exposure and should increase the

high temperature durability. It also should have refractive index close to glass in order to increase number photons which are emitted by nanocrystals, pass through the glass matrix. Among the available polymer films, polycarbonate films was the most suitable choice due to its refractive index and relatively low glass transition and drawing temperatures comparing to other counterparts. After this choice, during doping procedure, the mixture of nanocrystals and dissolved polymer should be as homogeneous as possible. For this reason, the mixture was well mixed taking hours of mixing and sonicated before pouring to the mold. The results was quite successful for going to next step. However, for the doping step, further improvement can be done in order to get more homogeneous films. This can be realized with making surface modifications to nanocrystals in order to avoid precipitation and agglomeration [68]. Yet, for the sake of simplicity, we leaved such a homogenization process to a future work. Also, we may use larger molds and more dopant for larger and condensed films. Furthermore, it should be noted that the method used for the nanocrystal doping is suitable for another dopant and another film. Thus, large-area doped polymer films can be built with easily with the method used for nanocrystal doping. In summary, we may say that the produced films were sufficiently homogeneous for going for the next step and the improvements and replacements can be topic of an another work.

The most crucial and challenging part was the production of the doped preform from doped films since we should realize a predetermined geometry and the preparation should not effect the luminescence of the dopant nanocrystals. For this reason, as we report in Chapter 4, we tried several geometries and finally a cylindrical doped core produced with a new technique which was originally developed. It consists of stacking circularly cut doped films and consolidation under mechanical pressure with predetermined cylindrical mold. With this new technique any cylindrical preform with any radius or length can be produced. It should be note that, for this procedure, the time requirement is a drawback but the success rate is quite high. Alternative methods are available such as PMMA powders/dopant mixture consolidation, but it limits the freedom of choice of the polymer. Also, development of new technique is an important part of a original research. The time consumption can be reduced with automation of the

procedure.

The procedure also allows producing other geometries such as rectangular or triangular preforms since the procedure mainly depends on shape of the cutter and the mold. For the production of the doped core step, further improvements with determining radius with calculations and simulations can be made for increasing emission efficiency and for wave-guiding/radial emitting. However, in this work we only focused on production, since with this production ability we can get any desired doped preforms with any radius or length. Hence, for the future research and new devices which uses core/cladding geometries, we demonstrated a new method and realized it with this work.

The rest of the production of the nanowires was two step thermal drawing which was used for many polymer and glass sets in our research group before this work [8]. After lots of experiences, most of the critical considerations about iterative thermal drawing were mastered. With this experience and knowledge, we applied the technique for our current design and we got successful result and produced the silicon nanocrystal doped luminescent nanowires. Hence, we also showed that silicon nanocrystal or other similar dopant doped nanowires or nanowire arrays can be produced with iterative thermal size reduction technique.

For this work, we only focused on production of the doped nanowires but the results showed us that the method is suitable for device development and further research. For example, a fiber laser with gain medium built from such a nanocrystal doped fibers can be realized with suitable geometry. With a suitable engineering of the doped material and the geometry, we can built a similar fiber laser with our production technique. A high efficient, high gain fiber amplifier or laser is already built from a double clad fiber [76]. In addition to double clad design, it is possible to design a photonic crystals structure with embedded light source and with engineering this structure it is possible to built fiber amplifiers or lasers. Also, for research purposes, single photon extraction is important topic and in literature there are already works which uses doped/structured nanowires in order to extract and guide photons [74]. Hence, our geometry and nanowires are also suitable for such processes. In summary, the fibers produced with ISR are

suitable both for potential applications and for future research. The next thing we will do about this research, can be development of a device like mentioned above but it requires long time since it should be designed more carefully and it will be a topic of another work.

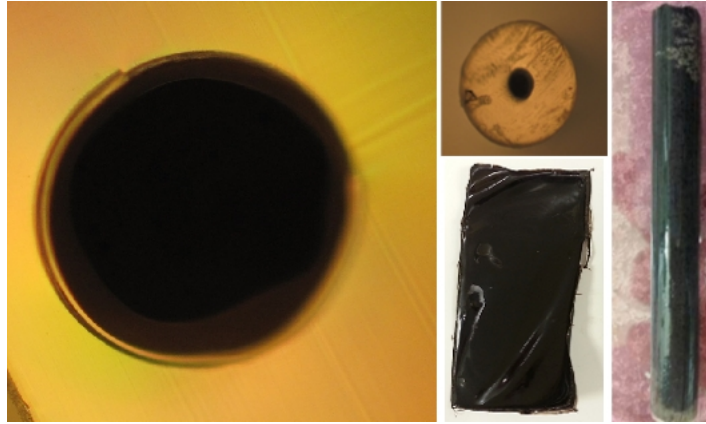


Figure 5.1: Iron nanoparticle doped films, preforms and fibers produced with the methods used in this work. The images shows that the methods are also suitable for other type of dopants and polymers rather than material sets used in this work. (Courtesy of Dr. Gökçen Birlik Demirel)

In conclusion, throughout this work we showed that with iterative size reduction method luminescent material doped nanowires can be produced. Actually, with this method, not only this type of dopant but also other types of dopant can be embedded in nanowires which was also realized for magnetic nanoparticles (Figure 5.1). The resultant nanowires were pictured and the luminescence were measured and interpreted with corresponding analysis. At this current level, the work shows its great potential for future improvements and applications. However, for this work we were contented with showing the applicability of the method which fulfills our proposals for this work. As mentioned throughout the work, with improvements in each production step, the success of the design can be increased drastically which opens new gates for potential research and technologies. The design may pave a way for elastic displays, fiber lasers, optic sensors *etc.* From the first time to very end, the relevant choices gave us a new method for production of structured nanofibers which may lead new research areas and technologies. Our next task may be to carry over the design to next level with designing such a proposed application which needs more time than this work and

more careful considerations. If we sum the whole work with a final word, a strong base was laid down and the new floors can be built with imagination and hard work.

Bibliography

- [1] M. Noginov, G. Zhu, A. Belgrave, R. Bakker, V. Shalaev, E. Narimanov, S. Stout, E. Herz, T. Suteewong, and U. Wiesner, “Demonstration of a spaser-based nanolaser,” *Nature*, vol. 460, no. 7259, pp. 1110–1112, 2009.
- [2] R. Bardhan, N. K. Grady, and N. J. Halas, “Nanoscale control of near-infrared fluorescence enhancement using au nanoshells,” *Small*, vol. 4, no. 10, pp. 1716–1722, 2008.
- [3] F. Tang, F. He, H. Cheng, and L. Li, “Self-assembly of conjugated polymer-ag@ SiO₂ hybrid fluorescent nanoparticles for application to cellular imaging,” *Langmuir*, vol. 26, no. 14, pp. 11774–11778, 2010.
- [4] W. Deng, D. Jin, K. Drozdowicz-Tomsia, J. Yuan, J. Wu, and E. M. Goldys, “Ultrabright eu-doped plasmonic ag@ sio2 nanostructures: Time-gated bioprobes with single particle sensitivity and negligible background,” *Adv. Mater.*, vol. 23, no. 40, pp. 4649–4654, 2011.
- [5] S. Schlecht, S. Tan, M. Yosef, R. Dersch, J. H. Wendorff, Z. Jia, and A. Schaper, “Toward linear arrays of quantum dots via polymer nanofibers and nanorods,” *Chem. Mater.*, vol. 17, no. 4, pp. 809–814, 2005.
- [6] N. Tomczak, S. Gu, M. Han, N. F. van Hulst, and G. Julius Vancso, “Single light emitters in electrospun polymer nanofibers: Effect of local confinement on radiative decay,” *Eur. Polym. J.*, vol. 42, no. 10, pp. 2205–2210, 2006.
- [7] H. Yu, R. Zhang, and B. Li, “Optical properties of quantum-dot-decorated polymer nanofibers,” *Nanotechnology*, vol. 22, no. 33, p. 335202, 2011.

- [8] M. Yaman, T. Khudiyev, E. Ozgur, M. Kanik, O. Aktas, E. O. Ozgur, H. Deniz, E. Korkut, and M. Bayindir, "Arrays of indefinitely long uniform nanowires and nanotubes," *Nat. Mater.*, vol. 10, no. 7, pp. 494–501, 2011.
- [9] J. K. Jaiswal, H. Mattoussi, J. M. Mauro, and S. M. Simon, "Long-term multiple color imaging of live cells using quantum dot bioconjugates," *Nat. Biotechnol.*, vol. 21, no. 1, pp. 47–51, 2002.
- [10] I. L. Medintz, H. T. Uyeda, E. R. Goldman, and H. Mattoussi, "Quantum dot bioconjugates for imaging, labelling and sensing," *Nat. Mater.*, vol. 4, no. 6, pp. 435–446, 2005.
- [11] E. Mutlugun, P. L. Hernandez-Martinez, C. Eroglu, Y. Coskun, T. Erdem, V. K. Sharma, E. Unal, S. K. Panda, S. G. Hickey, N. Gaponik, *et al.*, "Large-area (over 50 cm \times 50 cm) freestanding films of colloidal inp/zns quantum dots," *Nano Lett.*, vol. 12, no. 8, pp. 3986–3993, 2012.
- [12] E. Jang, S. Jun, H. Jang, J. Lim, B. Kim, and Y. Kim, "White-light-emitting diodes with quantum dot color converters for display backlights," *Adv. Mater.*, vol. 22, no. 28, pp. 3076–3080, 2010.
- [13] Q. Wang, Y. Bao, X. Zhang, P. R. Coxon, U. A. Jayasooriya, and Y. Chao, "Uptake and toxicity studies of poly-acrylic acid functionalized silicon nanoparticles in cultured mammalian cells," *Adv. Healthcare Mater.*, vol. 1, no. 2, pp. 189–198, 2012.
- [14] K. Dohnalová, L. Ondic, K. Kusová, I. Pelant, J. Rehspringer, and R.-R. Mafouana, "White-emitting oxidized silicon nanocrystals: Discontinuity in spectral development with reducing size," *J. Appl. Phys.*, vol. 107, no. 5, pp. 053102–053102, 2010.
- [15] C. M. Hessel, E. J. Henderson, and J. G. Veinot, "Hydrogen silsesquioxane: A molecular precursor for nanocrystalline si-sio₂ composites and freestanding hydride-surface-terminated silicon nanoparticles," *Chem. Mater.*, vol. 18, no. 26, pp. 6139–6146, 2006.

- [16] F. Gu, H. Yu, P. Wang, Z. Yang, and L. Tong, “Light-emitting polymer single nanofibers via waveguiding excitation,” *ACS Nano*, vol. 4, no. 9, pp. 5332–5338, 2010.
- [17] F. Di Benedetto, A. Camposeo, S. Pagliara, E. Mele, L. Persano, R. Stabile, R. Cingolani, and D. Pisignano, “Patterning of light-emitting conjugated polymer nanofibres,” *Nat. Nanotechnol.*, vol. 3, no. 10, pp. 614–619, 2008.
- [18] H. Yang, C. R. Lightner, and L. Dong, “Light-emitting coaxial nanofibers,” *ACS Nano*, vol. 6, no. 1, pp. 622–628, 2011.
- [19] L. Persano, A. Camposeo, F. Di Benedetto, R. Stabile, A. M. Laera, E. Piscopiello, L. Tapfer, and D. Pisignano, “Cds–polymer nanocomposites and light-emitting fibers by in situ electron-beam synthesis and lithography,” *Adv. Mater.*, vol. 24, no. 39, pp. 5320–5326, 2012.
- [20] J. S. Atchison and C. L. Schauer, “Fabrication and characterization of electrospun semiconductor nanoparticle—polyelectrolyte ultra-fine fiber composites for sensing applications,” *Sensors*, vol. 11, no. 11, pp. 10372–10387, 2011.
- [21] X. Xing, Y. Wang, and B. Li, “Nanofibers drawing and nanodevices assembly in poly (trimethylene terephthalate),” *Opt. Express*, vol. 16, no. 14, pp. 10815–10822, 2008.
- [22] O. Shapira, K. Kuriki, N. D. Orf, A. F. Abouraddy, G. Benoit, J. F. Viens, A. Rodriguez, M. Ibanescu, J. D. Joannopoulos, Y. Fink, *et al.*, “Surface-emitting fiber lasers,” *Opt. Express*, vol. 14, no. 9, pp. 3929–3935, 2006.
- [23] M. Fujiwara, K. Toubaru, T. Noda, H.-Q. Zhao, and S. Takeuchi, “Highly efficient coupling of photons from nanoemitters into single-mode optical fibers,” *Nano Lett.*, vol. 11, no. 10, pp. 4362–4365, 2011.
- [24] T. Takagahara and K. Takeda, “Theory of the quantum confinement effect on excitons in quantum dots of indirect-gap materials,” *Phys. Rev. B*, vol. 46, no. 23, p. 15578, 1992.
- [25] P. Harrison and P. Harrison, *Quantum wells, wires, and dots: theoretical and computational physics*, vol. 1. John Wiley & Sons New York, 2000.

- [26] W. F. Inc., “Quantum dot,” July 2013.
- [27] L. Pavesi and R. Turan, *Silicon Nanocrystals*. Wiley-VCh, 2010.
- [28] “Plasmachem gmbh zn/cdse/s alloyed quantum dots, url=<http://www.plasmachem.com/shop/en/226-zncdses-alloyed-quantum-dots>.”
- [29] A. Ekimov and A. Onushchenko, “Quantum size effect in three-dimensional microscopic semiconductor crystals,” *SPIE MILESTONE SERIES MS*, vol. 180, p. 3, 2005.
- [30] X. Michalet, F. F. Pinaud, L. A. Bentolila, J. M. Tsay, S. Doose, J. J. Li, G. Sundaresan, A. M. Wu, S. S. Gambhir, and S. Weiss, “Quantum dots for live cells, in vivo imaging, and diagnostics,” *Science*, vol. 307, no. 5709, pp. 538–544, 2005.
- [31] W. K. Leutwyler, S. L. Bürgi, and H. Burgl, “Semiconductor clusters, nanocrystals, and quantum dots,” *Science*, vol. 271, p. 933, 1996.
- [32] A. el Ahmedi, *Quantum Dots- A Variety of New Applications*, vol. 1. Intech, 2012.
- [33] Y. He, H.-T. Lu, L.-M. Sai, W.-Y. Lai, Q.-L. Fan, L.-H. Wang, and W. Huang, “Microwave-assisted growth and characterization of water-dispersed cdte/cds core-shell nanocrystals with high photoluminescence,” *J. Phys. Chem. B*, vol. 110, no. 27, pp. 13370–13374, 2006.
- [34] R. E. Bailey and S. Nie, “Alloyed semiconductor quantum dots: tuning the optical properties without changing the particle size,” *J. Am. Chem. Soc.*, vol. 125, no. 23, pp. 7100–7106, 2003.
- [35] K.-H. Lee, J.-H. Lee, W.-S. Song, H. Ko, C. Lee, J.-H. Lee, and H. Yang, “Highly efficient, color-pure, color-stable blue quantum dot light-emitting devices,” *ACS Nano*, vol. 0, no. 0, p. null, 2013.
- [36] C. Seydel, “Quantum dots get wet,” *Science*, vol. 300, no. 5616, pp. 80–81, 2003.

- [37] P. V. Kamat, “Quantum dot solar cells. the next big thing in photovoltaics,” *J. Phys. Chem. Lett.*, vol. 4, no. 6, pp. 908–918, 2013.
- [38] M. R. Krames, O. B. Shchekin, R. Mueller-Mach, G. O. Mueller, L. Zhou, G. Harbers, and M. G. Craford, “Status and future of high-power light-emitting diodes for solid-state lighting,” *J. Disp. Technol.*, vol. 3, no. 2, pp. 160–175, 2007.
- [39] H.-S. Chen, C.-K. Hsu, and H.-Y. Hong, “Ingan-cdse-znse quantum dots white leds,” *Photon. Technol. Lett., IEEE*, vol. 18, no. 1, pp. 193–195, 2006.
- [40] G. Yusa and H. Sakaki, “Trapping of photogenerated carriers by inas quantum dots and persistent photoconductivity in novel gaas/n-algaas field-effect transistor structures,” *Appl. Phys. Lett.*, vol. 70, no. 3, pp. 345–347, 1997.
- [41] D. Tu, S. Pagliara, A. Camposeo, L. Persano, R. Cingolani, and D. Pisignano, “Single light-emitting polymer nanofiber field-effect transistors,” *Nanoscale*, vol. 2, pp. 2217–2222, 2010.
- [42] D. Huffaker, G. Park, Z. Zou, O. Shchekin, and D. Deppe, “1.3 μm room-temperature gaas-based quantum-dot laser,” *Appl. Phys. Lett.*, vol. 73, no. 18, pp. 2564–2566, 1998.
- [43] D. S. Wiersma, P. Bartolini, A. Lagendijk, and R. Righini, “Localization of light in a disordered medium,” *Nature*, vol. 390, no. 6661, pp. 671–673, 1997.
- [44] P. Thomas, M. Möller, R. Eichmann, T. Meier, T. Stroucken, and A. Knorr, “Microscopic foundation of the förster excitonic energy transfer process,” *Phys. Status Solidi B*, vol. 230, no. 1, pp. 25–29, 2002.
- [45] M. Bashouti, W. Salalha, M. Brumer, E. Zussman, and E. Lifshitz, “Alignment of colloidal cds nanowires embedded in polymer nanofibers by electrospinning,” *ChemPhysChem*, vol. 7, no. 1, pp. 102–106, 2006.
- [46] H. Liu, J. B. Edel, L. M. Bellan, and H. Craighead, “Electrospun polymer nanofibers as subwavelength optical waveguides incorporating quantum dots,” *Small*, vol. 2, no. 4, pp. 495–499, 2006.

- [47] H. C. Y. Yu, A. Argyros, G. Barton, M. A. van Eijkelenborg, C. Barbe, K. Finnie, L. Kong, F. Ladouceur, and S. McNiven, “Quantum dot and silica nanoparticle doped polymer optical fibers,” *Opt. Express*, vol. 15, pp. 9989–9994, Aug 2007.
- [48] H. Yu, D. Liao, M. B. Johnston, and B. Li, “All-optical full-color displays using polymer nanofibers,” *ACS Nano*, vol. 5, no. 3, pp. 2020–2025, 2011.
- [49] M. Bayindir, F. Sorin, A. F. Abouraddy, J. Viens, S. D. Hart, J. D. Joannopoulos, and Y. Fink, “Metal–insulator–semiconductor optoelectronic fibres,” *Nature*, vol. 431, no. 7010, pp. 826–829, 2004.
- [50] P. Russell, “Photonic crystal fibers,” *Science*, vol. 299, no. 5605, pp. 358–362, 2003.
- [51] M. van Eijkelenborg, M. Large, A. Argyros, J. Zagari, S. Manos, N. Issa, I. Bassett, S. Fleming, R. McPhedran, C. M. de Sterke, and N. A. Nicorovici, “Microstructured polymer optical fibre,” *Opt. Express*, vol. 9, pp. 319–327, Sep 2001.
- [52] A. Abouraddy, M. Bayindir, G. Benoit, S. Hart, K. Kuriki, N. Orf, O. Shapira, F. Sorin, B. Temelkuran, and Y. Fink, “Towards multimaterial multifunctional fibres that see, hear, sense and communicate,” *Nat. Mater.*, vol. 6, no. 5, pp. 336–347, 2007.
- [53] F. Di Benedetto, A. Camposeo, L. Persano, A. M. Laera, E. Piscopiello, R. Cingolani, L. Tapfer, and D. Pisignano, “Light-emitting nanocomposite cds–polymer electrospun fibres via in situ nanoparticle generation,” *Nanoscale*, vol. 3, no. 10, pp. 4234–4239, 2011.
- [54] S. Godefroo, M. Hayne, M. Jivanescu, A. Stesmans, M. Zacharias, O. Lebedev, G. Van Tendeloo, and V. V. Moshchalkov, “Classification and control of the origin of photoluminescence from si nanocrystals,” *Nat. Nanotechnol.*, vol. 3, no. 3, pp. 174–178, 2008.
- [55] M. Henini, *Handbook of self assembled semiconductor nanostructures for novel devices in photonics and electronics*. Elsevier Science, 2011.

- [56] L. Canham, “Silicon quantum wire array fabrication by electrochemical and chemical dissolution of wafers,” *Appl. Phys. Lett.*, vol. 57, p. 1046, 1990.
- [57] T. Van Buuren, L. Dinh, L. Chase, W. Siekhaus, and L. J. Terminello, “Changes in the electronic properties of si nanocrystals as a function of particle size,” *Phys. Rev. Lett.*, vol. 80, no. 17, 1998.
- [58] M. Wolkin, J. Jorne, P. Fauchet, G. Allan, and C. Delerue, “Electronic states and luminescence in porous silicon quantum dots: the role of oxygen,” *Phys. Rev. Lett.*, vol. 82, no. 1, p. 197, 1999.
- [59] L. Mangolini, “Synthesis properties and applications of silicon nanocrystals,” *J. Vac. Sci. Technol. B*, vol. 31, no. 2, p. 29, 2013.
- [60] F. Maier-Flaig, J. Rinck, M. Stephan, T. Bocksrocker, M. Bruns, C. Kübel, A. K. Powell, G. A. Ozin, and U. Lemmer, “Multicolor silicon light-emitting diodes (sileds),” *Nano Lett.*, vol. 13, no. 2, pp. 475–480, 2013.
- [61] E.-C. Cho, S. Park, X. Hao, D. Song, G. Conibeer, S.-C. Park, and M. A. Green, “Silicon quantum dot/crystalline silicon solar cells,” *Nanotechnology*, vol. 19, no. 24, p. 245201, 2008.
- [62] A. Dutta, S. Oda, Y. Fu, and M. Willander, “Electron transport in nanocrystalline si based single electron transistors,” *J. J. Appl. Phys.*, vol. 39, no. Part 1, No. 7B, pp. 4647–4650, 2000.
- [63] A. Kenyon, C. Chryssou, C. Pitt, T. Shimizu-Iwayama, D. Hole, N. Sharma, and C. Humphreys, “Luminescence from erbium-doped silicon nanocrystals in silica: Excitation mechanisms,” *J. Appl. Phys.*, vol. 91, no. 1, pp. 367–374, 2002.
- [64] A. Mimura, M. Fujii, S. Hayashi, D. Kovalev, and F. Koch, “Photoluminescence and free-electron absorption in heavily phosphorus-doped si nanocrystals,” *Phys. Rev. B*, vol. 62, no. 19, p. 12625, 2000.
- [65] S. Tiwari, F. Rana, H. Hanafi, A. Hartstein, E. F. Crabbé, and K. Chan, “A silicon nanocrystals based memory,” *Appl. Phys. Lett.*, vol. 68, p. 1377, 1996.

- [66] J. Heitmann, F. Müller, M. Zacharias, and U. Gösele, “Silicon nanocrystals: Size matters,” *Adv. Mater.*, vol. 17, no. 7, pp. 795–803, 2005.
- [67] C. M. Hessel, M. R. Rasch, J. L. Hueso, B. W. Goodfellow, V. A. Akhavan, P. Puvanakrishnan, J. W. Tunnel, and B. A. Korgel, “Alkyl passivation and amphiphilic polymer coating of silicon nanocrystals for diagnostic imaging,” *Small*, vol. 6, no. 18, pp. 2026–2034, 2010.
- [68] C. M. Hessel, D. Reid, M. G. Panthani, M. R. Rasch, B. W. Goodfellow, J. Wei, H. Fujii, V. Akhavan, and B. A. Korgel, “Synthesis of ligand-stabilized silicon nanocrystals with size-dependent photoluminescence spanning visible to near-infrared wavelengths,” *Chem. Mater.*, vol. 24, no. 2, pp. 393–401, 2011.
- [69] M. Zacharias, J. Heitmann, R. Scholz, U. Kahler, M. Schmidt, and J. Blasing, “Size-controlled highly luminescent silicon nanocrystals: A SiO/SiO₂ superlattice approach,” *Appl. Phys. Lett.*, vol. 80, no. 4, pp. 661–663, 2002.
- [70] H. Tetsuka, T. Ebina, and F. Mizukami, “Highly luminescent flexible quantum dot–clay films,” *Adv. Mater.*, vol. 20, no. 16, pp. 3039–3043, 2008.
- [71] M. C. Neves, M. A. Martins, P. C. Soares-Santos, P. Rauwel, R. A. Ferreira, T. Monteiro, L. D. Carlos, and T. Trindade, “Photoluminescent, transparent and flexible di-ureasil hybrids containing cdse/zns quantum dots,” *Nanotechnology*, vol. 19, no. 15, p. 155601, 2008.
- [72] J. M. Cariou, J. Dugas, L. Martin, and P. Michel, “Refractive-index variations with temperature of pmma and polycarbonate,” *Appl. Opt.*, vol. 25, pp. 334–336, Feb 1986.
- [73] A. M. Stolyarov, L. Wei, O. Shapira, F. Sorin, S. L. Chua, J. D. Joannopoulos, and Y. Fink, “Microfluidic directional emission control of an azimuthally polarized radial fibre laser,” *Nat. Photonics*, vol. 6, no. 4, pp. 229–233, 2012.
- [74] J. Claudon, J. Bleuse, N. S. Malik, M. Bazin, P. Jaffrennou, N. Gregersen, C. Sauvan, P. Lalanne, and J.-M. Gérard, “A highly efficient single-photon source based on a quantum dot in a photonic nanowire,” *Nat. Photonics*, vol. 4, no. 3, pp. 174–177, 2010.

- [75] W. Wadsworth, J. Knight, W. H. Reeves, P. Russell, and J. Arriaga, “Yb³⁺-doped photonic crystal fibre laser,” *Electron. Lett.*, vol. 36, no. 17, pp. 1452–1454, 2000.
- [76] D. Kouznetsov and J. V. Moloney, “Highly efficient, high-gain, short-length, and power-scalable incoherent diode slab-pumped fiber amplifier/laser,” *J. Quantum Electron., IEEE*, vol. 39, no. 11, pp. 1452–1461, 2003.
- [77] Y. Zhao, C. Riemersma, F. Pietra, R. Koole, C. de Mello Donegà, and A. Meijerink, “High-temperature luminescence quenching of colloidal quantum dots,” *ACS Nano*, vol. 6, no. 10, pp. 9058–9067, 2012.
- [78] S. F. Wuister, C. de Mello Donegá, and A. Meijerink, “Luminescence temperature anti-quenching of water-soluble CdTe quantum dots: role of the solvent,” *J. Am. Chem. Soc.*, vol. 126, no. 33, pp. 10397–10402, 2004.

Appendix A

Data

Appendix B

Code